

Computing singlet scalar freeze-out with plasmon and plasmino states

S. Biondini^a, M. Eriksson^b, M. Laine^b

^a*Institute of Physics, University of Freiburg,
Hermann-Herder-Straße 3, 79014 Freiburg, Germany*

^b*AEC, Institute for Theoretical Physics, University of Bern,
Sidlerstrasse 5, CH-3012 Bern, Switzerland*

Abstract

The final-state particles from cosmological dark matter co-annihilation are expected to equilibrate. As dictated by Hard Thermal Loop resummation, the spectrum of equilibrated quasi-particles is richer than in vacuum, with a massless gauge field possessing three independent polarization states (“plasmons”), and a massless fermion developing a novel branch (“plasmino”). Furthermore, once the Higgs phenomenon sets in, vacuum and thermal mass corrections interfere. We collect together the corresponding poles and residues for the Standard Model around its crossover temperature. Choosing its singlet scalar extension for illustration, we subsequently demonstrate, both numerically and via power counting, and in accordance with general theoretical expectations, how in the freeze-out of TeV-scale dark matter, these effects remain well hidden in the inclusive annihilation cross section. In particular, the dominant (longitudinal) gauge channel is shown to be practically temperature-independent. Cosmological constraints on TeV-scale singlet scalars are reconfirmed.

Emails: `simone.biondini@physik.uni-freiburg.de`, `magdalena.eriksson@unibe.ch`, `laine@itp.unibe.ch`

Contents

1	Introduction	1
2	Formulation of the problem	4
3	Feynman rules, contractions, and gauge invariance	5
3.1	Feynman rules for the HTL-resummed Standard Model	5
3.2	Diagrams for a retarded singlet scalar self-energy	12
3.3	Cancellation of gauge parts	13
3.4	Physical parts	14
4	Cuts of self-energy diagrams	15
4.1	A prototypical example	15
4.2	Choice of kinematic variables	17
4.3	Results for the high-temperature phase ($T > T_c$)	19
4.4	Results for the HTL-resummed WW channel in the Higgs phase ($T < T_c$) . .	19
5	Phenomenological determination of dark matter abundance	23
6	Conclusions	25
A	Two-particle phase space integral	27
B	Leading-order matrix elements squared in the unresummed limit	28
C	HTL-resummed ZZ channel	30
D	HTL-resummed $t\bar{t}$ channel	32

1. Introduction

The relic density of cold dark matter, obtained by fitting Planck data to the standard cosmological model, is given by $\Omega_{\text{dm}} h^2 = 0.120 \pm 0.001$ [1]. This precise measurement imposes a strong constraint on the nature of dark matter and on the mechanism by which it is formed. In the freeze-out scenario [2,3], dark matter is at first in equilibrium with a thermal plasma. As the universe cools down, the dark matter density should become Boltzmann-suppressed. Dynamically, the density can decrease via $2 \rightarrow 2$ co-annihilation processes. However, once the co-annihilation rate becomes smaller than the Hubble rate, the decrease terminates, and dark matter falls out of equilibrium. By combining tools from quantum field theory and non-equilibrium statistical physics, the corresponding relic density $\Omega_{\text{dm}} h^2$ can be computed

theoretically, as a function of the parameters of a given model. In principle, we should aim at a similar 1% precision in these computations as on the observational side.

Of course, as long as the nature of dark matter is unknown, the majority of the literature concentrates on model building rather than on precision computations. That said, it is also appreciated that in some cases, the non-equilibrium physics responsible for the freeze-out process becomes non-trivial [4, 5]. In concrete terms, we may wonder about the correct functional form of the kinetic equations to be used, as well as about the radiative and thermal corrections that affect the “matching coefficients” that parametrize the kinetic equations.

A unifying theoretical framework for computing radiative and thermal corrections to the matching coefficients (at least in a class of theories) has been formulated only rather recently. A key insight is that to understand the structure of the matching coefficients, we should place ourselves on the side of the dark matter, viewing the Standard Model plasma as a heat bath, whose microscopic details do not need to be resolved. Then the matching coefficients can be related to “spectral functions” of the portal operators by which dark matter decays. The structure of the spectral functions can, in turn, be analyzed through the framework of the operator product expansion, as was first shown in the context of QCD [6]. This way, thermal corrections can be shown to be powerlike, with the powers dictated by the dimensions of gauge-invariant condensates. In the cosmological context, this type of computations were first carried out for non-relativistic leptogenesis [7–9], where thermal corrections go like T^2 , and subsequently also for specific dark matter scenarios [10, 11].

However, wonderful as a unifying framework is, one can still have second thoughts. One is that the low-temperature expansion in powers of T^2 is asymptotic, and in fact shows poor convergence [12]. A second is that whereas the cosmological freeze-out process is fully “inclusive”, if we instead think about dark matter direct or indirect detection, or its production at colliders, we are forced to consider specific “exclusive” Standard Model channels.¹ Would it not be nice to understand the freeze-out dynamics in the same language?

If we do adopt an exclusive viewpoint, the problem rapidly becomes complicated. Concretely, for weakly interacting TeV-scale dark matter, freeze-out happens close to the temperature of the electroweak crossover. Then masses induced by the Higgs mechanism ($\sim gv$) are of the same order as thermal mass corrections ($\sim gT$). In thermal field theory, these are known as *soft scales*. If the physics that we are considering is sensitive to the soft scales, perturbative computations need to be “resummed”, through the framework of Hard Thermal Loop effective theories [13–16]. Often, a further challenge is that it may not be transparent in advance which scales really matter. Then we may be tempted to resum “just in case”. The goal of the present investigation is related to such an approach: we would like to demonstrate, as pedagogically as possible, that such an exclusive viewpoint, including resummations, is also

¹In an *inclusive* process, only the initial state is specified, and all possible final states are included. In an *exclusive* process, the final-state particles and their kinematics are specified as well.

viable, and in the end only leads to very small thermal corrections, even if intermediate steps get substantially modified compared with a vacuum-like computation.

Given that our main focus is on a formal side, we have decided to adopt one of the simplest marginally viable dark matter scenarios for illustration, obtained through the addition of a gauge-singlet scalar field to the Standard Model [17–23]. This model has been employed for illustration purposes before. One example is if the singlet scalar mass happens to be about 1/2 of the Higgs mass. Then dark matter can annihilate via a resonant mechanism with extremely small couplings [24–28], which are not experimentally excluded [29, 30]. Another possibility could be if the mass and couplings are pushed to become large. Then the dark matter particles become strongly interacting, with associated effects like a Sommerfeld enhancement of their co-annihilation cross section [31] (though this is likely screened by the non-zero Higgs mass). A further non-trivial scenario originates if the singlet scalar converts the electroweak phase transition into a first-order one (cf., e.g., refs. [32, 33]).

In the present paper, we inspect a region of the parameter space in which *no* exotic phenomena are expected, and a standard analysis should suffice. Notably, we consider singlet scalar vacuum masses $m_{\varphi, \text{phys}} \sim$ a few TeV and couplings $\kappa \sim 1$, which were mildly favoured by global fits some time ago [22, 23].² The question we pose is whether a resummed computation, with its new channels, could yield larger thermal effects than generally expected, particularly if the freeze-out takes place close to the electroweak crossover? Though the results yield no surprises, the details do reveal a rich and partly unexplored structure, which might find use in other contexts as well.

Our paper is organized as follows. Given the fact that our computation leads us to some technical detail, we start by outlining the approach on a general level, in sec. 2. The computation itself can then be factorized into two main parts. First, in sec. 3, we establish the Feynman rules for the Hard Thermal Loop resummed Standard Model, and use them to compute a particular 2-point function of the dark matter field. At this stage, many cancellations can be verified, notably that of gauge independence, providing for an important crosscheck. In the second part, in sec. 4, we extract the “cut”, or imaginary part, of the 2-point correlator, which is proportional to the annihilation cross section. At this stage, tedious phase-space integrals are met, but given that cancellations had already taken place, the set that needs to be tackled is the minimal one. The phase-space constraints permit us to set up a power counting, establishing the importance of various contributions. The results are inserted into a practical dark matter freeze-out computation in sec. 5, before we conclude in sec. 6. Further details related to sec. 4 are relegated into four appendices.

²It is appropriate to remark that, given the theoretical nature of our work, we have *not* applied the latest rather stringent constraints from the observational side. A recent look at the strongly interacting regime of the singlet scalar model, in light of direct detection updates, can be found in ref. [34].

2. Formulation of the problem

If we want to compute thermally averaged dark matter annihilation cross sections beyond leading order in couplings, or if we want to “re-sum” effects from arbitrarily high loop orders, the conventional Boltzmann equations do *not* offer for a robust starting point. The particles appearing in them are vacuum-like asymptotic scattering states. However, within a medium, through Hard Thermal Loop (HTL) corrections [13–16], particles develop thermal masses and thermal interaction rates. Moreover, the number of physical polarization states, defined through the on-shell energies that can be found for a given momentum, increases from that in vacuum, opening up new channels. In order to account for these effects, we need to replace the Boltzmann equations through a quantum field theoretic framework.

A relatively simple way to establish a well-defined starting point is to relate the annihilation cross section appearing in a Boltzmann equation to an *equilibration rate*. The benefit of equilibration rates is that they have an unambiguous physical meaning within the linear response regime, and can therefore be computed with any formalism, including thermal quantum field theory. Specifically, as we are interested in inelastic reactions changing particle number, we should be concerned with a chemical equilibration rate [35].

The chemical equilibration rate can be viewed as a subpart of what has been called a maximal interaction rate [36]. For the maximal interaction rate, a simple recipe can be formulated. Suppose that we write the dark matter field φ as $\varphi \rightarrow \tilde{\varphi} + \varphi$, where $\tilde{\varphi}$ is treated as a kinetically equilibrated mode, and φ as an out-of-equilibrium mode. The terms linear in φ in the action can be expressed as

$$S \supset \int_X \varphi(X) \mathcal{O}(X) = \not\!\!\!\int_K \varphi(K) \mathcal{O}(-K), \quad (2.1)$$

where we employ the imaginary-time formalism, denoting the corresponding four-momentum by $K = (\omega_n, \mathbf{k})$ and the sum-integral by $\not\!\!\!\int_K \equiv T \sum_{\omega_n} \int_{\mathbf{k}}$. Let us then compute the self-energy of the φ particle,

$$\Pi_{K;\varphi} \equiv \left\langle \mathcal{O}(-K) \not\!\!\!\int_Q \mathcal{O}(Q) \right\rangle. \quad (2.2)$$

Once the frequency is analytically continued to a Minkowskian one, $\omega_n \rightarrow -i[\omega + i0^+]$, the Euclidean self-energy turns into a retarded self-energy. Its imaginary part (“cut”) defines the maximal interaction rate,

$$\Gamma_{\mathcal{K};\varphi}^{\max} \equiv \frac{\text{Im } \Pi_{\mathcal{K};\varphi}}{\omega}, \quad \mathcal{K} \equiv (\omega, \mathbf{k}), \quad \omega \equiv \sqrt{k^2 + m_\varphi^2}, \quad k \equiv |\mathbf{k}|, \quad (2.3)$$

where the momentum subscript \mathcal{K} indicates that analytic continuation has been carried out.

We note in passing that in ref. [37], a rate was obtained just like in eq. (2.3), and its physical relevance was rigorously established in a context in which a single φ -field is weakly coupled to the Standard Model. Here, our physical context is different, in that originally the

coupling of φ to Standard Model fields could be quadratic. The linear appearance of eq. (2.1) has only emerged after the shift $\varphi \rightarrow \varphi + \tilde{\varphi}$.

Once $\Gamma_{\mathcal{K};\varphi}^{\max}$ has been computed, we would like to obtain the corresponding annihilation cross section. As a first step, we need to select the contribution of the inelastic processes to the rate, writing

$$\Gamma_{\mathcal{K};\varphi}^{\max} \equiv \Gamma_{\mathcal{K};\varphi}^{\text{inel}} + \Gamma_{\mathcal{K};\varphi}^{\text{elas}} . \quad (2.4)$$

The inelastic processes are those in which, in addition to φ , at least one $\tilde{\varphi}$ is pulled to the initial state. In total, $\Gamma_{\mathcal{K};\varphi}^{\text{inel}}$ can be represented as a sum of i dark matter particles in the initial state, $\Gamma_{\mathcal{K};\varphi}^{\text{inel}} = \sum_{i \geq 2} \Gamma_{\mathcal{K};\varphi}^{\text{inel}(i)}$. In the non-relativistic regime, $i = 2$ gives the dominant contribution, up to corrections suppressed by $e^{-m_\varphi/T} \ll 1$. Subsequently, we can average over momenta, whereby the contribution of the elastic processes drops out. Assuming kinetic equilibrium, so that the momenta of the dark matter particles follow the Bose distribution, denoted by f_B , this yields

$$\langle \sigma v_{\text{rel}} \rangle \equiv \frac{\int_{\mathbf{k}} \Gamma_{\mathcal{K};\varphi}^{\text{inel}(2)} f_B(\omega)}{n_{\text{eq}}^2} , \quad (2.5)$$

where the number density has been expressed as

$$n_{\text{eq}} \equiv \int_{\mathbf{k}} f_B(\omega) . \quad (2.6)$$

Even though we have given these as definitions, it can be verified that in the regime of validity of Boltzmann equations, eq. (2.5) agrees with the corresponding averaged cross section (cf. sec. 4). Then the rate equation also has the familiar form [38],

$$(\partial_t + 3H)n_\varphi \approx -\langle \sigma v_{\text{rel}} \rangle (n_\varphi^2 - n_{\text{eq}}^2) . \quad (2.7)$$

3. Feynman rules, contractions, and gauge invariance

3.1. Feynman rules for the HTL-resummed Standard Model

We would now like to compute the self-energy in eq. (2.2). For this, we need the Feynman rules for the Standard Model extended by the singlet scalar field. Specifically, we assume the singlet scalar to be heavy, with a mass of a few TeV. Then its decoupling takes place at temperatures close to those of the electroweak crossover, $T \simeq 160$ GeV [39]. The Standard Model gauge bosons, scalars, and fermions are “soft” in this regime, with vacuum masses in general smaller than the “hard” thermal scale, $\sim \pi T$. Then the Feynman rules need to be worked out in the context of a HTL effective theory.³ Previously, soft real-time physics in the

³In general, the HTL theory involves both propagator and vertex corrections. However, the vertices of a scalar particle do not get corrected, and since in our case the singlet scalar communicates with the Standard Model through the Higgs field, we do not need to worry about the vertex corrections.

same temperature regime has been considered, for instance, for low-scale leptogenesis [40,41] or for the equilibration rate of the Standard Model Higgs field [42,43].

The theory considered is defined by the Lagrangian

$$\mathcal{L} = \mathcal{L}_{SM} + \left\{ \frac{1}{2} \partial^\mu \varphi \partial_\mu \varphi - \left[\frac{1}{2} m_{\varphi 0}^2 \varphi^2 + \frac{1}{2} \kappa \varphi^2 H^\dagger H + \frac{1}{4} \lambda_\varphi \varphi^4 \right] \right\}, \quad (3.1)$$

where H is the Standard Model Higgs doublet. After electroweak symmetry breaking, the Higgs doublet can be written as

$$H = \begin{pmatrix} G_w \\ \frac{1}{\sqrt{2}} [v + h + iG_z] \end{pmatrix}, \quad (3.2)$$

where the normalization is such that the expectation value in vacuum reads $v|_{T=0} \simeq 246$ GeV. The scalar singlet is assumed to be heavy in the sense that $m_{\varphi 0}^2 \gg \kappa v^2|_{T=0}$.

At finite temperature, the value of v gets reduced. However, v is a delicate quantity, first of all because it is gauge dependent, and second, because it is sensitive to soft ($\sim gT$) [44] and even ultrasoft ($\sim g^2 T/\pi$) [45] scales. The latter issue can be rephrased by noting that the Higgs mass parameter, m_h^2 , receives a correction $\sim (g^2 T/\pi)^2$, where part of the coefficient is non-perturbative. In order to handle this issue, which in the end is not important for our theoretical considerations, even though it plays a visible numerical role, we make use of a lattice determination of the pseudocritical temperature $T_c \simeq 160$ GeV of the Standard Model crossover [39]. With its help, we parametrize $v \equiv v|_T \simeq v|_{T=0} \text{Re} \sqrt{1 - T^2/T_c^2}$. For the benefit of readers wishing to apply our formalism to BSM frameworks for which no lattice input is available, we remark that our main results remain practically unchanged even if an approximate perturbative evaluation of $v|_T$ is employed. In terms of diagrams, the evolution of v corresponds to effects originating from tadpole diagrams, i.e. those that would contribute to $\langle h \rangle$. As their effects have been accounted for through v , we have $\langle h \rangle \simeq 0$, and tadpole diagrams are omitted from our actual computation.

As for the singlet scalar, in a thermal environment its mass becomes

$$m_\varphi^2 \approx m_{\varphi 0}^2 + \kappa \left(\frac{v^2}{2} + \frac{T^2}{6} \right). \quad (3.3)$$

Here the T^2 -part is strictly speaking correct only for $\pi T \gg m_h$, but we do not need to worry about this, since in the opposite limit the thermal correction is subdominant to the v^2 -part. The physical mass at $T = 0$ is

$$m_{\varphi, \text{phys}}^2 \stackrel{(3.3)}{\underset{T=0}{\approx}} m_{\varphi 0}^2 + \frac{\kappa v^2}{2} \Big|_{T=0}. \quad (3.4)$$

For the electroweak sector, we work in a general R_ξ gauge, with the gauge parameter denoted by ξ . Apart from the Higgs field (h , illustrated with dashed lines) and the heavy

singlet ($\tilde{\varphi}$, illustrated with solid lines), the particles playing a role in the loops are the charged and neutral Goldstone modes (G_W and G_Z , illustrated with dashed lines), the charged and neutral ghosts (c_W , c_Z , illustrated with dotted lines), the gauge bosons (W , Z , illustrated with wiggly lines), and the fermions (t , b , illustrated with arrowed lines). The corresponding tree-level physical masses in the thermal ground state are $m_W^2 = g_2^2 v^2/4$, $m_Z^2 = (g_1^2 + g_2^2)v^2/4$, $m_t^2 = h_t^2 v^2/2$, $m_b^2 = h_b^2 v^2/2$ where g_1 and g_2 are the U(1) and SU(2) gauge couplings, respectively, and h_t and h_b are the top and bottom Yukawa couplings. The masses of the Goldstones ($m_{G_{W,Z}}^2$), longitudinal gauge field polarizations ($m_{W,Z}^{\prime 2}$), and ghosts ($m_{W,Z}^{\prime 2}$) agree, $m_{G_W}^2 \equiv m_W^{\prime 2} \equiv \xi m_W^2$ and $m_{G_Z}^2 \equiv m_Z^{\prime 2} \equiv \xi m_Z^2$. For the Higgs excitation, we adopt a different notation according to whether the Higgs mechanism is active or not,

$$m_h^2 \simeq \frac{m_{h,\text{phys}}^2}{2} \left(\frac{T^2}{T_c^2} - 1 \right) + 3\lambda_h v^2 \stackrel{T \leq T_c}{=} 2\lambda_h v^2 = m_{h,\text{phys}}^2 \left(1 - \frac{T^2}{T_c^2} \right), \quad (3.5)$$

$$m_\phi^2 \stackrel{T > T_c}{\simeq} \frac{m_{h,\text{phys}}^2}{2} \left(\frac{T^2}{T_c^2} - 1 \right), \quad (3.6)$$

where v is the thermally modified Higgs expectation value and $m_{h,\text{phys}} \approx 125$ GeV. To be clear, we remark that eq. (3.6) is directly the (resummed) mass parameter appearing in the effective Lagrangian, whereas in the low-temperature result of eq. (3.5), the value of v needs to be chosen so that we find ourselves in the Higgs minimum.

The propagators of the HTL-resummed theory are simple for the spin-0 particles,

$$\Delta_{P;h}^{-1} \equiv \frac{1}{P^2 + m_h^2}, \quad \Delta_{P;\tilde{\varphi}}^{-1} \equiv \frac{1}{P^2 + m_\phi^2}, \quad (3.7)$$

$$\Delta_{P;G_{W,Z}}^{-1} \equiv \frac{1}{P^2 + m_{W,Z}^{\prime 2}}, \quad \Delta_{P;c_{W,Z}}^{-1} \equiv \frac{1}{P^2 + m_{W,Z}^{\prime 2}}. \quad (3.8)$$

For the gauge sector, we need the transverse (T), longitudinal (L), and electric (E) projectors,

$$\mathbb{P}_{\mu\nu}^T \equiv \delta_{\mu i} \delta_{\nu j} \left(\delta_{ij} - \frac{p_i p_j}{p^2} \right), \quad \mathbb{P}_{\mu\nu}^L \equiv \frac{P_\mu P_\nu}{P^2}, \quad \mathbb{P}_{\mu\nu}^E \equiv \delta_{\mu\nu} - \mathbb{P}_{\mu\nu}^T - \mathbb{P}_{\mu\nu}^L, \quad (3.9)$$

where $p \equiv |\mathbf{p}|$. The corresponding HTL self-energies will ultimately be employed after analytic continuation, so it is helpful to list those expressions already,

$$\Pi_{(-i(p^0+i0^+),\mathbf{p})}^{Tj} = \frac{m_{Ej}^2}{2} \left\{ \frac{(p^0)^2}{p^2} + \frac{p^0}{2p} \left[1 - \frac{(p^0)^2}{p^2} \right] \ln \frac{p^0 + p + i0^+}{p^0 - p + i0^+} \right\}, \quad (3.10)$$

$$\widehat{\Pi}_{(-i(p^0+i0^+),\mathbf{p})}^{Ej} = \frac{m_{Ej}^2}{p^2} \left[1 - \frac{p^0}{2p} \ln \frac{p^0 + p + i0^+}{p^0 - p + i0^+} \right], \quad (3.11)$$

where $j \in \{1, 2\}$, and the thermal masses read

$$m_{E1}^2 = \left(\frac{n_S}{6} + \frac{5n_G}{9} \right) g_1^2 T^2 + \mathcal{O}(g_1^4), \quad m_{E2}^2 = \left(\frac{2}{3} + \frac{n_S}{6} + \frac{n_G}{3} \right) g_2^2 T^2 + \mathcal{O}(g_2^4), \quad (3.12)$$

where $n_s \equiv 1$ is the number of Higgs doublets and $n_G \equiv 3$ the number of fermion generations. Furthermore, for the electric part, we have written the original self-energy in a rescaled form,

$$\Pi_P^E \equiv P^2 \hat{\Pi}_P^E. \quad (3.13)$$

With the given self-energies, propagators can be worked out. It is helpful to recombine the structures appearing in them so that only a single pole appears in each part. In the charged gauge boson sector, this leads to

$$[\Delta_{P;W}^{-1}]_{\mu\nu} = [\Delta_{P;W}^{-1}]_{\mu\nu}^{\text{phys}} - \frac{P_\mu P_\nu}{m_W^2(P^2 + m_W^2)}, \quad (3.14)$$

$$[\Delta_{P;W}^{-1}]_{\mu\nu}^{\text{phys}} \equiv \mathbb{P}_{\mu\nu}^T \mathcal{G}_P^T + (\delta_{\mu\nu} - \mathbb{P}_{\mu\nu}^T) \mathcal{G}_P^E + \frac{P_\mu P_\nu}{m_W^2} \hat{\mathcal{G}}_P^E, \quad (3.15)$$

$$\mathcal{G}_P^T \equiv \frac{1}{P^2 + \Pi_P^{T2} + m_W^2}, \quad (3.16)$$

$$\mathcal{G}_P^E \equiv \frac{1}{P^2(1 + \hat{\Pi}_P^{E2}) + m_W^2}, \quad (3.17)$$

$$\hat{\mathcal{G}}_P^E \equiv \frac{1 + \hat{\Pi}_P^{E2}}{P^2(1 + \hat{\Pi}_P^{E2}) + m_W^2}. \quad (3.18)$$

The situation is more complicated in the neutral sector. We employ sign conventions in which the covariant derivative acting on the Higgs doublet reads

$$D_\mu H = \left(\partial_\mu + \frac{ig_1 B_\mu}{2} - ig_2 T^a A_\mu^a \right) H, \quad T^a \equiv \frac{\sigma^a}{2}, \quad (3.19)$$

where σ^a are the Pauli matrices. The vacuum mixing angles are defined as

$$s \equiv \frac{g_1}{\sqrt{g_1^2 + g_2^2}}, \quad c \equiv \frac{g_2}{\sqrt{g_1^2 + g_2^2}}. \quad (3.20)$$

In the basis of the original (Lagrangian) gauge fields, the quadratic part of the HTL effect action contains

$$S \supset \oint_P \frac{1}{2} \begin{pmatrix} A_{\mu;-P}^3 \\ B_{\mu;-P} \end{pmatrix}^T \begin{pmatrix} M_{AA} & M_{AB} \\ M_{AB} & M_{BB} \end{pmatrix} \begin{pmatrix} A_{\mu;P}^3 \\ B_{\mu;P} \end{pmatrix}, \quad (3.21)$$

$$M_{AA} = \delta_{\mu\nu}(P^2 + c^2 m_Z^2) - P_\mu P_\nu + \frac{P_\mu P_\nu}{\xi} + \mathbb{P}_{\mu\nu}^T \Pi_P^{T2} + \mathbb{P}_{\mu\nu}^E \Pi_P^{E2}, \quad (3.22)$$

$$M_{AB} = \delta_{\mu\nu} c s m_Z^2, \quad (3.23)$$

$$M_{BB} = \delta_{\mu\nu}(P^2 + s^2 m_Z^2) - P_\mu P_\nu + \frac{P_\mu P_\nu}{\xi} + \mathbb{P}_{\mu\nu}^T \Pi_P^{T1} + \mathbb{P}_{\mu\nu}^E \Pi_P^{E1}. \quad (3.24)$$

With the help of projectors from eq. (3.9), we can split eq. (3.21) into three independent parts. Each of them can be inverted separately. Subsequently, we can rotate into the basis of the vacuum-like fields,

$$\begin{pmatrix} A_{\mu;P}^3 \\ B_{\mu;P} \end{pmatrix} = \begin{pmatrix} c & -s \\ s & c \end{pmatrix} \begin{pmatrix} Z_{\mu;P} \\ Q_{\mu;P} \end{pmatrix}. \quad (3.25)$$

We only need the ZZ component from the propagator matrix. Furthermore, the terms proportional to $P_\mu P_\nu$ from $\mathbb{P}_{\mu\nu}^E$ (cf. eq. (3.9)) can be combined with those from $\mathbb{P}_{\mu\nu}^L$, in order to remove spurious poles. This way, we obtain an expression analogous to that in eqs. (3.14) and (3.15),

$$[\Delta_{P;Z}^{-1}]_{\mu\nu} = [\Delta_{P;Z}^{-1}]_{\mu\nu}^{\text{phys}} - \frac{P_\mu P_\nu}{m_Z^2(P^2 + m_Z'^2)}, \quad (3.26)$$

$$[\Delta_{P;Z}^{-1}]_{\mu\nu}^{\text{phys}} = \mathbb{P}_{\mu\nu}^T \mathcal{F}_P^T + (\delta_{\mu\nu} - \mathbb{P}_{\mu\nu}^T) \mathcal{F}_P^E + \frac{P_\mu P_\nu}{m_Z^2} \hat{\mathcal{F}}_P^E, \quad (3.27)$$

$$\mathcal{F}_P^T \equiv \frac{P^2 + c^2 \Pi_P^{T1} + s^2 \Pi_P^{T2}}{(P^2 + \Pi_P^{T1})(P^2 + \Pi_P^{T2}) + m_Z^2(P^2 + c^2 \Pi_P^{T1} + s^2 \Pi_P^{T2})}, \quad (3.28)$$

$$\mathcal{F}_P^E \equiv \frac{1 + c^2 \hat{\Pi}_P^{E1} + s^2 \hat{\Pi}_P^{E2}}{P^2(1 + \hat{\Pi}_P^{E1})(1 + \hat{\Pi}_P^{E2}) + m_Z^2(1 + c^2 \hat{\Pi}_P^{E1} + s^2 \hat{\Pi}_P^{E2})}, \quad (3.29)$$

$$\hat{\mathcal{F}}_P^E \equiv \frac{1 - m_Z^2 \mathcal{F}_P^E}{P^2} = \frac{(1 + \hat{\Pi}_P^{E1})(1 + \hat{\Pi}_P^{E2})}{P^2(1 + \hat{\Pi}_P^{E1})(1 + \hat{\Pi}_P^{E2}) + m_Z^2(1 + c^2 \hat{\Pi}_P^{E1} + s^2 \hat{\Pi}_P^{E2})}. \quad (3.30)$$

If we set $s^2 \rightarrow 0$, $c^2 \rightarrow 1$, the charged propagators in eqs. (3.16)–(3.18) are reproduced.

Turning finally to fermions (in practice we only consider quarks, which have the largest Yukawa couplings), the action has a similar matrix structure as in eq. (3.21). With the example of top quarks, and denoting $t_{L,R} \equiv a_{L,R} t$, where $a_{L,R} \equiv (\mathbb{1} \mp \gamma_5)/2$ are the chiral projectors, the quadratic part of the HTL effective action reads

$$S \supset \not\!\!\!\int_{\{P\}} (\bar{t}_L \bar{t}_R) \begin{pmatrix} \not{L}_{\mathcal{P}} & m_t \\ m_t & \not{R}_{\mathcal{P}} \end{pmatrix} \begin{pmatrix} t_L \\ t_R \end{pmatrix}, \quad (3.31)$$

where $\not\!\!\!\int_{\{P\}}$ denotes a fermionic Matsubara sum-integral. The four-vectors L and R , introduced in ref. [46], have the forms

$$\not{L}_{\mathcal{P}} = L_{\mathcal{P};\mu} \gamma^\mu, \quad (3.32)$$

$$L_{\mathcal{P};\mu} \equiv \{p_0 (1 + c_{\mathcal{P};t_L}^W), p_i (1 + c_{\mathcal{P};t_L}^P)\}, \quad (3.33)$$

and similarly for $L \rightarrow R$, where we have already gone over to Minkowskian Dirac matrices and carried out a Wick rotation (in Minkowskian spacetime we use the metric signature $+- - -$). Here the HTL self-energies, the analogues of eq. (3.10) and (3.11), read

$$c_{\mathcal{P};t_L}^{\text{W}} \equiv -\frac{m_{t_L}^2}{2pp^0} \ln \frac{p^0 + p + i0^+}{p^0 - p + i0^+}, \quad (3.34)$$

$$c_{\mathcal{P};t_L}^{\text{P}} \equiv \frac{m_{t_L}^2}{p^2} \left[1 - \frac{p^0}{2p} \ln \frac{p^0 + p + i0^+}{p^0 - p + i0^+} \right], \quad (3.35)$$

and similarly with $L \rightarrow R$. For top and bottom quarks, the thermal mass parameters read (cf., e.g., ref. [47])

$$m_{t_L}^2 = m_{b_L}^2 \approx T^2 \left(\frac{g_1^2}{288} + \frac{3g_2^2}{32} + \frac{g_3^2}{6} + \frac{h_t^2 + h_b^2}{16} \right), \quad (3.36)$$

$$m_{t_R}^2 \approx T^2 \left(\frac{g_1^2}{18} + \frac{g_3^2}{6} + \frac{h_t^2}{8} \right), \quad m_{b_R}^2 \approx T^2 \left(\frac{g_1^2}{72} + \frac{g_3^2}{6} + \frac{h_b^2}{8} \right). \quad (3.37)$$

The inversion of the matrix from eq. (3.31) was worked out in ref. [46]. Showing the chiral projectors explicitly, the result can be written as

$$\begin{aligned} \mathbb{A}_{\mathcal{P};t}^{-1} = & \mathcal{F}_{\mathcal{P}}^t \left\{ a_L (R_{\mathcal{P}}^2 \not{L}_{\mathcal{P}} - m_t^2 \not{R}_{\mathcal{P}}) a_R - a_L m_t \left(L_{\mathcal{P}} \cdot R_{\mathcal{P}} - m_t^2 + \frac{[\not{L}_{\mathcal{P}}, \not{R}_{\mathcal{P}}]}{2} \right) a_L \right. \\ & \left. + a_R (L_{\mathcal{P}}^2 \not{R}_{\mathcal{P}} - m_t^2 \not{L}_{\mathcal{P}}) a_L - a_R m_t \left(L_{\mathcal{P}} \cdot R_{\mathcal{P}} - m_t^2 - \frac{[\not{L}_{\mathcal{P}}, \not{R}_{\mathcal{P}}]}{2} \right) a_R \right\}, \quad (3.38) \end{aligned}$$

$$\mathcal{F}_{\mathcal{P}}^t \equiv \frac{1}{L_{\mathcal{P}}^2 R_{\mathcal{P}}^2 - 2m_t^2 L_{\mathcal{P}} \cdot R_{\mathcal{P}} + m_t^4}. \quad (3.39)$$

We note that if we only keep the contribution from the SU(3) coupling g_3^2 in eqs. (3.36)–(3.37), which is the largest individual term, then the thermal masses of the chiral states agree with each other. In this situation, the quarks are vectorlike, with $L = R$. Consequently the propagator from eqs. (3.38) and (3.39) can be greatly simplified,

$$\mathbb{A}_{\mathcal{P};t}^{-1} \stackrel{L \rightarrow R}{=} \frac{m_t \mathbb{1} - p_0 \gamma^0 (1 + c_{\mathcal{P}}^{\text{W}}) - p_i \gamma^i (1 + c_{\mathcal{P}}^{\text{P}})}{\Delta_{\mathcal{P};t}}, \quad (3.40)$$

$$\Delta_{\mathcal{P};t} \equiv m_t^2 + p^2 (1 + c_{\mathcal{P}}^{\text{P}})^2 - (p^0)^2 (1 + c_{\mathcal{P}}^{\text{W}})^2, \quad (3.41)$$

where the thermal masses appearing in $c_{\mathcal{P}}^{\text{W}}$ and $c_{\mathcal{P}}^{\text{P}}$ (cf. eqs. (3.34) and (3.35)) are now defined by retaining only the SU(3) parts of eqs. (3.36) and (3.37),

$$m_{t_{L=R}}^2 \equiv \frac{g_3^2 T^2}{6}. \quad (3.42)$$

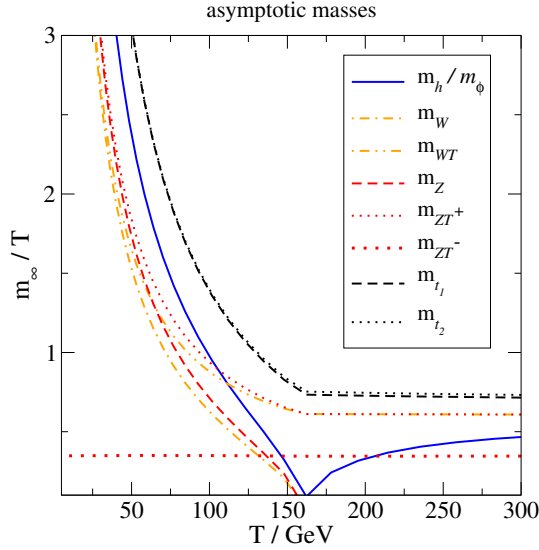



Figure 1: An illustration of the asymptotic masses in various channels: m_h and m_ϕ , from eqs. (3.5) and (3.6); m_W and m_{WT} , from eqs. (4.28) and (4.29); m_Z , m_{ZT+} and m_{ZT-} , from eqs. (C.1) and (C.3); and m_{t_1} and m_{t_2} , from eq. (D.6). We remark that m_{WT} and m_{ZT+} become degenerate at $T > T_c$, reflecting the absence of a Higgs mechanism, whereas m_{ZT-} represents the thermal asymptotic mass of a photon or hypercharge excitation.


We end this subsection by stressing that when HTL corrections are included, the spin- $\frac{1}{2}$ and spin-1 propagators that we are faced with (eqs. (3.16)–(3.18) for W , eqs. (3.28)–(3.30) for Z , eqs. (3.38)–(3.41) for t) are non-polynomial functions of p^0 and p . In this situation there is no unambiguous notion of a “mass”; rather, a dispersion relation, if defined as a location of a pole, depends on the spatial momentum in a non-covariant way. As will become apparent later on (cf. discussion around eq. (4.23)), for our problem relevant are hard momenta, $p \gg \pi T$. Then we can parametrize dispersion relations by what are called *asymptotic masses*, as $p^0 \approx p + m_\infty^2/(2p) + \mathcal{O}(1/p^3)$. The asymptotic masses can be defined in all cases, but there are more channels than in vacuum, with the W splitting into two channels (with asymptotic masses m_W^2 and m_{WT}^2 , cf. eqs. (4.28) and (4.29)); the Z splitting into three channels (with the asymptotic masses m_Z^2 and $m_{ZT\pm}^2$, cf. eqs. (C.1) and (C.3)); and the t splitting into two channels (with the asymptotic masses $m_{t_1}^2$ and $m_{t_2}^2$, cf. eq. (D.6)). We illustrate the numerical magnitudes of these asymptotic masses in fig. 1, together with the effective Higgs mass, m_h at $T < T_c$ from eq. (3.5) and m_ϕ at $T > T_c$ from eq. (3.6).

3.2. Diagrams for a retarded singlet scalar self-energy


Making use of the notation introduced in sec. 3.1, and suppressing sum-integration symbols, the contributions of the various diagrams to the self-energy defined in eq. (2.2) read




$$\Pi_{K;\varphi} \supset \frac{\kappa^2}{2} \Delta_{-K-P;\tilde{\varphi}}^{-1} \left\{ \Delta_{Q;h}^{-1} \Delta_{P-Q;h}^{-1} \right. \\ \left. + \Delta_{Q;G_z}^{-1} \Delta_{P-Q;G_z}^{-1} + 2 \Delta_{Q;G_w}^{-1} \Delta_{P-Q;G_w}^{-1} \right\}, \quad (3.43)$$




$$\Pi_{K;\varphi} \supset -\kappa^2 m_h^2 \Delta_{-K-P;\tilde{\varphi}}^{-1} \Delta_{P;h}^{-1} \left\{ 3 \Delta_{Q;h}^{-1} \Delta_{P-Q;h}^{-1} \right. \\ \left. + \Delta_{Q;G_z}^{-1} \Delta_{P-Q;G_z}^{-1} + 2 \Delta_{Q;G_w}^{-1} \Delta_{P-Q;G_w}^{-1} \right\}, \quad (3.44)$$




$$\Pi_{K;\varphi} \supset \frac{\kappa^2 m_h^4}{2} \Delta_{-K-P;\tilde{\varphi}}^{-1} \Delta_{P;h}^{-2} \left\{ 9 \Delta_{Q;h}^{-1} \Delta_{P-Q;h}^{-1} \right. \\ \left. + \Delta_{Q;G_z}^{-1} \Delta_{P-Q;G_z}^{-1} + 2 \Delta_{Q;G_w}^{-1} \Delta_{P-Q;G_w}^{-1} \right\}, \quad (3.45)$$




$$\Pi_{K;\varphi} \supset -2\kappa^3 v^2 \Delta_{-K-P;\tilde{\varphi}}^{-1} \Delta_{-K-Q;\tilde{\varphi}}^{-1} \Delta_{P;h}^{-1} \Delta_{P-Q;h}^{-1}, \quad (3.46)$$




$$\Pi_{K;\varphi} \supset 3\kappa^3 v^2 m_h^2 \Delta_{-K-P;\tilde{\varphi}}^{-1} \Delta_{-K-Q;\tilde{\varphi}}^{-1} \Delta_{P;h}^{-1} \Delta_{Q;h}^{-1} \Delta_{P-Q;h}^{-1}, \quad (3.47)$$




$$\Pi_{K;\varphi} \supset \kappa^4 v^4 \Delta_{-K-P;\tilde{\varphi}}^{-1} \Delta_{Q;\tilde{\varphi}}^{-1} \Delta_{P-Q;\tilde{\varphi}}^{-1} \Delta_{-K-Q;h}^{-1} \Delta_{P;h}^{-1}, \quad (3.48)$$



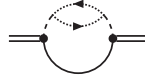
$$\Pi_{K;\varphi} \supset \kappa^4 v^4 \Delta_{-K-P;\tilde{\varphi}}^{-2} \Delta_{P-Q;\tilde{\varphi}}^{-1} \Delta_{-K-Q;h}^{-1} \Delta_{P;h}^{-1}, \quad (3.49)$$




$$\Pi_{K;\varphi} \supset \kappa^2 \Delta_{-K-P;\tilde{\varphi}}^{-1} \Delta_{P;h}^{-2} (P_\mu + Q_\mu)(P_\nu + Q_\nu) \left\{ \right. \\ \left. + \Delta_{Q;G_w}^{-1} [\Delta_{P-Q;W}^{-1}]_{\mu\nu} [2m_W^2] \right. \\ \left. + \Delta_{Q;G_z}^{-1} [\Delta_{P-Q;Z}^{-1}]_{\mu\nu} [m_Z^2] \right\}, \quad (3.50)$$



$$\Pi_{K;\varphi} \supset 2\kappa^2 \Delta_{-K-P;\tilde{\varphi}}^{-1} \Delta_{P;h}^{-2} \left\{ [\Delta_{Q;W}^{-1}]_{\mu\nu} [\Delta_{P-Q;W}^{-1}]_{\nu\mu} [2m_W^4] \right. \\ \left. + [\Delta_{Q;Z}^{-1}]_{\mu\nu} [\Delta_{P-Q;Z}^{-1}]_{\nu\mu} [m_Z^4] \right\}, \quad (3.51)$$



$$\Pi_{K;\varphi} \supset -\kappa^2 \Delta_{-K-P;\tilde{\varphi}}^{-1} \Delta_{P;h}^{-2} \left\{ \Delta_{Q;c_W}^{-1} \Delta_{P-Q;\tilde{c}_W}^{-1} [2m_W'^4] \right. \\ \left. + \Delta_{Q;c_Z}^{-1} \Delta_{P-Q;\tilde{c}_Z}^{-1} [m_Z'^4] \right\}, \quad (3.52)$$



$$\Pi_{K;\varphi} \supset -\kappa^2 N_c \Delta_{-K-P;\tilde{\varphi}}^{-1} \Delta_{P;h}^{-2} \left\{ m_t^2 \text{Tr} [\mathbb{A}_{Q;t}^{-1} \mathbb{A}_{Q-P;t}^{-1}] \right. \\ \left. + m_b^2 \text{Tr} [\mathbb{A}_{Q;b}^{-1} \mathbb{A}_{Q-P;b}^{-1}] \right\}. \quad (3.53)$$

3.3. Cancellation of gauge parts

An important consistency check of the computation is that all gauge dependence cancels. In terms of eqs. (3.43)–(3.53), this is equivalent to the disappearance of the masses m'_W and m'_Z . Such effects originate from the Goldstone propagators in eqs. (3.43), (3.44), (3.45) and (3.50); the longitudinal parts of the gauge propagators in eqs. (3.50) and (3.51); and the ghost propagators in eq. (3.52). Having written the gauge propagators in analogous forms in eqs. (3.14)–(3.15) and (3.26)–(3.30), respectively, the cancellation takes place in the same way in the charged and neutral sectors. For instance, collecting together the gauge terms of the charged sector, we find

$$\Pi_{K;\varphi} \supset \kappa^2 \Delta_{-K-P;\tilde{\varphi}}^{-1} \Delta_{P;h}^{-2} \Delta_{Q;G_W}^{-1} \Delta_{P-Q;G_W}^{-1} \left\{ \right. \\ \left. + (P^2 + m_h^2)^2 - 2m_h^2(P^2 + m_h^2) + m_h^4 - 2m_W'^4 \right. \\ \left. - 2(P_\mu + Q_\mu)(P_\nu + Q_\nu)(P_\mu - Q_\mu)(P_\nu - Q_\nu) \right. \\ \left. + 4Q_\mu Q_\nu(P_\mu - Q_\mu)(P_\nu - Q_\nu) \right\} \\ + 2\kappa^2 m_W^2 \Delta_{-K-P;\tilde{\varphi}}^{-1} \Delta_{P;h}^{-2} \Delta_{Q;G_W}^{-1} [\Delta_{P-Q;W}^{-1}]_{\mu\nu}^{\text{phys}} \left\{ \right. \\ \left. + (P_\mu + Q_\mu)(P_\nu + Q_\nu) - 4Q_\mu Q_\nu \right\}. \quad (3.54)$$

By completing squares in the first part, *viz.*

$$-2(P^2 - Q^2)^2 + 4(Q \cdot P - Q^2)^2 = 2m_W'^4 - P^4 \quad (3.55) \\ + \Delta_{P-Q;G_W}^2 + 2\Delta_{P-Q;G_W} \Delta_{Q;G_W} - \Delta_{Q;G_W}^2 - 2\Delta_{P-Q;G_W} [P^2 + 2m_W'^2] + 2\Delta_{Q;G_W} P^2,$$

we note that the terms on the first line of eq. (3.55) cancel against the second line of eq. (3.54), whereas the terms of the second line of eq. (3.55) remove at least one of the propagators, leaving over terms in which one loop is a tadpole, i.e. factorized from the rest. Such terms yield no cut corresponding to a $2 \rightarrow 2$ process. In the second part of eq. (3.54), after writing

simpler expression that can be obtained from eq. (3.40), *viz.*

$$\begin{aligned}
\text{Diagram} & \quad \Pi_{K;\varphi} \stackrel{L \rightarrow R}{\supset} 4\kappa^2 m_t^2 N_c \Delta_{-K-P;\tilde{\varphi}}^{-1} \Delta_{P;h}^{-2} \Delta_{Q;t}^{-1} \Delta_{Q-P;t}^{-1} \left\{ \right. \\
& \quad + \mathbf{q} \cdot (\mathbf{q} - \mathbf{p}) (1 + c_Q^P) (1 + c_{Q-P}^P) \\
& \quad \left. - q^0 (q^0 - p^0) (1 + c_Q^W) (1 + c_{Q-P}^W) - m_t^2 \right\}, \quad (3.58)
\end{aligned}$$

where the thermal mass appearing in c_Q^W and c_Q^P is defined via eq. (3.42).

4. Cuts of self-energy diagrams

Having determined the self-energy $\Pi_{K;\varphi}$ (cf. sec. 3.4), the next task is to analytically continue it to Minkowskian spacetime and then extract its imaginary part, or “cut”, $\text{Im } \Pi_{K;\varphi}$, which is what is needed in eq. (2.3) and then eq. (2.5). We illustrate here how this can be done, if we do not know *a priori* whether the final-state particles can be represented as on-shell excitations. This means that they will appear as general “spectral functions”, ϱ_Q (cf. eq. (4.3)).

4.1. A prototypical example

Let us consider a structure similar to what appears in the gauge contribution, eq. (3.56), but simplified to the core. Denoting by \mathcal{F} a resummed propagator, by Φ terms that will not be cut, and by $\delta(P)$ a Dirac-delta normalized as $\oint_P \delta(P) = 1$, we focus on

$$\begin{aligned}
I_K & \equiv \Delta_{-K-P;\tilde{\varphi}}^{-1} \mathcal{F}_Q \mathcal{F}_{P-Q} \Phi \\
& \equiv \oint_{P,Q} \frac{\mathcal{F}_Q \mathcal{F}_{P-Q} \Phi}{(K+P)^2 + m_\varphi^2} \\
P \equiv -H-K & \quad \oint_{H,Q} \frac{\mathcal{F}_Q \mathcal{F}_{-K-H-Q} \Phi}{H^2 + m_\varphi^2} = \oint_{H,Q,R} \delta(K+H+Q+R) \frac{\mathcal{F}_Q \mathcal{F}_R \Phi}{H^2 + m_\varphi^2} \\
\epsilon_h^2 \equiv h^2 + m_\varphi^2 & \quad \oint_{H,Q,R} \int_{-\infty}^{\infty} \frac{dq_0}{\pi} \int_{-\infty}^{\infty} \frac{dr_0}{\pi} \frac{\delta(K+H+Q+R)}{h_n^2 + \epsilon_h^2} \frac{\varrho_Q}{q_0 - iq_n} \frac{\varrho_R}{r_0 - ir_n} \Phi, \quad (4.2)
\end{aligned}$$

where we represented \mathcal{F}_Q in a spectral representation,

$$\mathcal{F}_Q = \int_{-\infty}^{\infty} \frac{dq_0}{\pi} \frac{\varrho_Q}{q_0 - iq_n}, \quad \varrho_Q \equiv \text{Im } \mathcal{F}_Q|_{q_n \rightarrow -i(q_0 + i0^+)}. \quad (4.3)$$

For free particles, spectral functions amount to localized “poles” (cf. eq. (4.8)), but more generally they are continuous “cuts”.

We now express the temporal part of $\delta(K + H + Q + R)$ as a Fourier integral, and carry out the Matsubara sums,

$$\begin{aligned}
I_K &= \int_{\mathbf{h}, \mathbf{q}, \mathbf{r}} \delta(\mathbf{k} + \mathbf{h} + \mathbf{q} + \mathbf{r}) \int_{-\infty}^{\infty} \frac{dq_0}{\pi} \int_{-\infty}^{\infty} \frac{dr_0}{\pi} \varrho_Q \varrho_R \Phi \\
&\times \int_0^\beta d\tau e^{ik_n \tau} \left\{ \underbrace{T \sum_{h_n} \frac{e^{ih_n \tau}}{h_n^2 + \epsilon_h^2}}_{\frac{f_B(\epsilon_h)}{2\epsilon_h} [e^{(\beta-\tau)\epsilon_h} + e^{\tau\epsilon_h}]} \right\} \left\{ \underbrace{T \sum_{q_n} \frac{e^{iq_n \tau}}{q_0 - iq_n}}_{f_B(q_0) e^{\tau q_0}} \right\} \left\{ \underbrace{T \sum_{r_n} \frac{e^{ir_n \tau}}{r_0 - ir_n}}_{f_B(r_0) e^{\tau r_0}} \right\} \\
&= \int_{\mathbf{h}, \mathbf{q}, \mathbf{r}} \delta(\mathbf{k} + \mathbf{h} + \mathbf{q} + \mathbf{r}) \int_{-\infty}^{\infty} \frac{dq_0}{\pi} \int_{-\infty}^{\infty} \frac{dr_0}{\pi} \varrho_Q \varrho_R \Phi \frac{f_B(\epsilon_h) f_B(q_0) f_B(r_0)}{2\epsilon_h} \\
&\times \left\{ \frac{e^{\beta(q_0+r_0)} - e^{\beta\epsilon_h}}{ik_n - \epsilon_h + q_0 + r_0} + \frac{e^{\beta(\epsilon_h+q_0+r_0)} - 1}{ik_n + \epsilon_h + q_0 + r_0} \right\}. \tag{4.4}
\end{aligned}$$

We then set $k_n \rightarrow -i(\omega + i0^+)$ and take the imaginary part, by making use of

$$\text{Im} \frac{1}{\Delta + i0^+} = -\pi \delta(\Delta). \tag{4.5}$$

This yields

$$\begin{aligned}
\text{Im} I_K &= \frac{1}{2} \int_{\mathbf{h}, \mathbf{q}, \mathbf{r}} \frac{\delta(\mathbf{k} + \mathbf{h} + \mathbf{q} + \mathbf{r})}{2\epsilon_h} \int_{-\infty}^{\infty} \frac{dq_0}{\pi} \int_{-\infty}^{\infty} \frac{dr_0}{\pi} \varrho_Q \varrho_R \Phi \\
&\times \left\{ 2\pi \delta(\omega - \epsilon_h + q_0 + r_0) [\bar{f}_B(\epsilon_h) f_B(q_0) f_B(r_0) - f_B(\epsilon_h) \bar{f}_B(q_0) \bar{f}_B(r_0)] \right. \\
&\quad \left. + 2\pi \delta(\omega + \epsilon_h + q_0 + r_0) [f_B(\epsilon_h) f_B(q_0) f_B(r_0) - \bar{f}_B(\epsilon_h) \bar{f}_B(q_0) \bar{f}_B(r_0)] \right\} \\
&\stackrel{\mathcal{Q} \rightarrow -\mathcal{Q}}{\underset{\mathcal{R} \rightarrow -\mathcal{R}}{=}} \frac{1}{2} \int_{\mathbf{h}, \mathbf{q}, \mathbf{r}} \frac{\delta(\mathbf{k} + \mathbf{h} - \mathbf{q} - \mathbf{r})}{2\epsilon_h} \int_{-\infty}^{\infty} \frac{dq_0}{\pi} \int_{-\infty}^{\infty} \frac{dr_0}{\pi} \varrho_Q \varrho_R \Phi \tag{4.6} \\
&\times \left\{ 2\pi \delta(\omega - \epsilon_h - q_0 - r_0) [\bar{f}_B(\epsilon_h) \bar{f}_B(q_0) \bar{f}_B(r_0) - f_B(\epsilon_h) f_B(q_0) f_B(r_0)] \right. \\
&\quad \left. + 2\pi \delta(\omega + \epsilon_h - q_0 - r_0) [f_B(\epsilon_h) \bar{f}_B(q_0) \bar{f}_B(r_0) - \bar{f}_B(\epsilon_h) f_B(q_0) f_B(r_0)] \right\},
\end{aligned}$$

where in the second step we made use of the (bosonic) properties

$$\varrho_{-Q} = -\varrho_Q, \quad f_B(-q_0) = -\bar{f}_B(q_0), \quad \bar{f}_B(q_0) \equiv 1 + f_B(q_0). \tag{4.7}$$

In order to understand which part of the large integration domain of eq. (4.6) is important, let us for a moment consider an unresummed propagator, with

$$\mathcal{F}_Q = \frac{1}{q_n^2 + \epsilon_q^2} \stackrel{(4.3)}{\Rightarrow} \varrho_Q = \frac{\pi}{2\epsilon_q} [\delta(q_0 - \epsilon_q) - \delta(q_0 + \epsilon_q)]. \tag{4.8}$$

If we insert this in eq. (4.6), the two channels there split into four different channels each, yielding in total eight possibilities, corresponding to $1 \rightarrow 3$, $2 \rightarrow 2$, $3 \rightarrow 1$, and a hypothetical $4 \rightarrow 0$ process. Among these, only the $2 \rightarrow 2$ ones are kinematically realized in the non-relativistic limit. Among the $2 \rightarrow 2$ channels, only one is relevant for the inelastic rate, namely that with φ and $\tilde{\varphi}$ in the initial state. This originates from the second row of eq. (4.6), with q_0 and r_0 taken positive. Furthermore, we note that

$$f_B(\epsilon_h) \bar{f}_B(q_0) \bar{f}_B(r_0) = f_B(\epsilon_h) f_B(q_0) f_B(r_0) e^{(q_0+r_0)/T}, \quad (4.9)$$

$$\bar{f}_B(\epsilon_h) f_B(q_0) f_B(r_0) = f_B(\epsilon_h) f_B(q_0) f_B(r_0) e^{\epsilon_h/T}. \quad (4.10)$$

Given that $q_0 + r_0 = \omega + \epsilon_h \gg \epsilon_h$, the first factor, which we may refer to as a loss term, dominates by an exponentially large amount over the gain term ($\omega/T \geq m_\varphi/T \gg 1$). Moreover, since q_0 and r_0 carry the energy released from the co-annihilation of φ and $\tilde{\varphi}$, each of them is large. Therefore, the final-state Bose enhancements, $f_B(q_0)$ and $f_B(r_0)$, are exponentially small, and can be omitted in practice, implying that $\bar{f}_B(q_0) \approx 1 \approx \bar{f}_B(r_0)$. Similarly, the initial-state factor $f_B(\epsilon_h)$, as well as the corresponding $f_B(\omega)$ from eq. (2.5), can be replaced by the leading terms in a dilute expansion,

$$f_B(\epsilon_h) \rightarrow e^{-\beta\epsilon_h}, \quad f_B(\omega) \rightarrow e^{-\beta\omega}. \quad (4.11)$$

Note that as long as we do not replace the energies by their non-relativistic limits, the dilute expansion is rapidly convergent. With these simplifications, eq. (4.6), with $\varrho_{\mathcal{Q}}$ and $\varrho_{\mathcal{R}}$ restored to their general forms, serves as the starting point for the next steps (cf. eq. (4.12)).

4.2. Choice of kinematic variables

Before we insert the spectral functions $\varrho_{\mathcal{Q}}$ and $\varrho_{\mathcal{R}}$ into eq. (4.6), it is helpful to rewrite the integration measure in terms of new variables. Starting from eqs. (2.5) and (4.6); making use of the simplifications explained between eqs. (4.10) and (4.11); and noting from eqs. (3.56)–(3.58) that the four-momenta appearing in the weight of the integrand can normally be expressed in terms of Q and $R \equiv P - Q$, which become \mathcal{Q} and \mathcal{R} after going over to the spectral representation, we consider an integral of the form

$$\begin{aligned} \langle \sigma v_{\text{rel}} \rangle & \stackrel{(2.5)}{\underset{(4.6),(4.11)}}{=} \frac{1}{n_{\text{eq}}^2} \int_{\mathbf{k}, \mathbf{h}, \mathbf{q}, \mathbf{r}} \int_{-\infty}^{\infty} \frac{dq_0}{\pi} \int_{-\infty}^{\infty} \frac{dr_0}{\pi} \frac{(2\pi)^4 \delta^{(4)}(\mathcal{K} + \mathcal{H} - \mathcal{Q} - \mathcal{R})}{4\omega\epsilon_h} \\ & \times \varrho_{\mathcal{Q}} \varrho_{\mathcal{R}} e^{-\beta(\omega+\epsilon_h)} \Phi(\mathcal{Q}, \mathcal{R}). \end{aligned} \quad (4.12)$$

We now re-introduce the center-of-mass four-momentum $\mathcal{P} = (p_0, \mathbf{p})$ and write

$$\delta^{(4)}(\mathcal{K} + \mathcal{H} - \mathcal{Q} - \mathcal{R}) = \int d^4\mathcal{P} \delta^{(4)}(\mathcal{K} + \mathcal{H} - \mathcal{P}) \delta^{(4)}(\mathcal{P} - \mathcal{Q} - \mathcal{R}). \quad (4.13)$$

Then we change the order of integrations, and consider the outer integral

$$I \equiv \int_{\mathbf{k}, \mathbf{h}} \frac{(2\pi)^4 \delta(\omega + \epsilon_h - p_0) \delta^{(3)}(\mathbf{k} + \mathbf{h} - \mathbf{p})}{4\omega \epsilon_h} = \int_{\mathbf{k}} \frac{2\pi \delta(\omega + \epsilon_{pk} - p_0)}{4\omega \epsilon_{pk}}, \quad (4.14)$$

where $\omega \equiv \sqrt{k^2 + m_\varphi^2}$ and $\epsilon_{pk} \equiv \sqrt{(\mathbf{p} - \mathbf{k})^2 + m_\varphi^2}$. The Dirac- δ can give a contribution if $p_0 > \sqrt{p^2 + 4m_\varphi^2}$. Rather than k , it is helpful to take ω as an integration variable, and then the integration boundaries can be established as

$$k_\pm \stackrel{\mathcal{P}^2 > 4m_\varphi^2}{=} \frac{p}{2} \pm \frac{p_0}{2} \sqrt{1 - \frac{4m_\varphi^2}{\mathcal{P}^2}} \Rightarrow \omega_\pm \stackrel{\mathcal{P}^2 > 4m_\varphi^2}{=} \frac{p_0}{2} \pm \frac{p}{2} \sqrt{1 - \frac{4m_\varphi^2}{\mathcal{P}^2}}, \quad (4.15)$$

where

$$\mathcal{P}^2 \equiv p_0^2 - p^2. \quad (4.16)$$

The integral over the angle between \mathbf{k} and \mathbf{p} can be carried out, with the Jacobian yielding $\epsilon_{pk}/(pk)$. Combining these steps, we find

$$I \stackrel{(4.14)}{\stackrel{(4.15)}{=}} \theta(p_0 - \sqrt{p^2 + 4m_\varphi^2}) \int_{\omega_-}^{\omega_+} \frac{d\omega}{8\pi p}. \quad (4.17)$$

Furthermore we note that in eq. (4.12), the exponential factor contains ω , but according to eq. (4.14), we can replace $\omega + \epsilon_h \rightarrow p_0$. Then the integrand is independent of ω , and the ω -integral can be trivially carried out. This finally yields a somewhat simpler representation for eq. (4.12),

$$\begin{aligned} \langle \sigma v_{\text{rel}} \rangle &\stackrel{(4.12)}{\stackrel{(4.17), (4.15)}{=}} \frac{1}{n_{\text{eq}}^2} \overbrace{\int d^3\mathbf{p}}^{4\pi \int_0^\infty dp p^2} \int_{\sqrt{p^2 + 4m_\varphi^2}}^\infty dp_0 \frac{e^{-\beta p_0} \sqrt{1 - \frac{4m_\varphi^2}{\mathcal{P}^2}}}{8\pi} \\ &\times \int_{\mathbf{q}, \mathbf{r}} \int_{-\infty}^\infty \frac{dq_0}{\pi} \int_{-\infty}^\infty \frac{dr_0}{\pi} \delta^{(4)}(\mathcal{P} - \mathcal{Q} - \mathcal{R}) \varrho_{\mathcal{Q}} \varrho_{\mathcal{R}} \Phi(\mathcal{Q}, \mathcal{R}). \end{aligned} \quad (4.18)$$

In eq. (4.18), \mathcal{P} is effectively the four-momentum of an off-shell Higgs boson. The formula indicates that we need to evaluate its $1 \rightarrow 2$ decays into Standard Model particles, with thermal effects contained in $\varrho_{\mathcal{Q}}$ and $\varrho_{\mathcal{R}}$ and in the “matrix element squared” $\Phi(\mathcal{Q}, \mathcal{R})$. The Higgs is *not* at rest with respect to the medium but, as follows from the thermal weight $e^{-\beta p_0}$, carries a typical momentum $p \sim \sqrt{m_\varphi T} \gg \pi T$.

We remark in passing that if we move towards the relativistic regime, i.e. $\pi T \gtrsim m_\varphi$, then it can happen that because of the thermal mass corrections experienced by Standard Model particles (cf. fig. 1), $m_\varphi \sim m_\phi$. In this situation the kinematics changes from what we have assumed above, most simply because it is not sufficient to have $p_0^2 - p^2 > 4m_\varphi^2$, but \mathcal{P}^2 also needs to be large enough to set the final-state particles on-shell (provided that their spectral functions are of the type in eq. (4.8)).

4.3. Results for the high-temperature phase ($T > T_c$)

Let us first apply the formalism to a simple example. For this we go to temperatures $T > T_c$, where most of the contributions drop out. The remaining result reads

$$\text{Diagram: a circle with two external lines on the left and a dashed line on top} \quad \lim_{v \rightarrow 0} \Pi_{K;\varphi} \supset \Delta_{-P-K;\tilde{\varphi}}^{-1} \Delta_{Q;\phi}^{-1} \Delta_{P-Q;\phi}^{-1} \overbrace{\{2\kappa^2\}}^{\equiv \Phi_{\phi\phi}}, \quad (4.19)$$

where ϕ denotes scalar excitations (with 4 real degrees of freedom).

Inserting unresummed spectral functions from eq. (4.8) into eq. (4.12), we obtain

$$\begin{aligned} \langle \sigma v_{\text{rel}} \rangle &\stackrel{(4.19)}{\approx} \stackrel{(4.8),(4.12)}{=} \frac{1}{n_{\text{eq}}^2} \int \frac{1}{(2\pi)^{12}} \frac{d^3\mathbf{k}}{2\omega} \frac{d^3\mathbf{h}_{\tilde{\varphi}}}{2\epsilon_{\tilde{\varphi}}} \frac{d^3\mathbf{q}_{\phi_1}}{2\epsilon_{\phi_1}} \frac{d^3\mathbf{r}_{\phi_2}}{2\epsilon_{\phi_2}} (2\pi)^4 \delta^{(4)}(\mathcal{K} + \mathcal{H}_{\tilde{\varphi}} - \mathcal{Q}_{\phi_1} - \mathcal{R}_{\phi_2}) \\ &\times e^{-\beta(\omega + \epsilon_{\tilde{\varphi}})} \{2\kappa^2\}. \end{aligned} \quad (4.20)$$

From here we see that $\Phi_{\phi\phi} = 2\kappa^2$ corresponds to the usual matrix element squared, summed over final-state degeneracies, and with a prefactor $1/2!$ to cancel the overcounting for the integration over the momenta of identical final-state particles, *viz.*

$$2\kappa^2 = \frac{1}{2!} 4 |\mathcal{M}|^2, \quad |\mathcal{M}| = \kappa. \quad (4.21)$$

For a practical integration, it is beneficial to proceed with eq. (4.18). The integrals over q_0 and r_0 can be carried out with the help of eq. (4.8). The phase-space integral over \mathbf{q} and \mathbf{r} can also be performed, as we recall in appendix A. Then we are left over with a three-dimensional integral, similar to eq. (4.33), which is rapidly convergent and easy to evaluate numerically.

4.4. Results for the HTL-resummed WW channel in the Higgs phase ($T < T_c$)

Our main challenge is to generalize the results to the Higgs phase, including contributions from the non-polynomial HTL self-energies. In the language of eqs. (4.12) and (4.13), the large initial-state energy $p_0 = \omega + \epsilon_h \geq 2m_\varphi$ is transmitted to the Standard Model energies, q_0 and r_0 . Moreover, because of the Boltzmann weight

$$e^{-\beta p_0} \leq e^{-\beta \sqrt{p^2 + 4m_\varphi^2}} \approx e^{-\beta [2m_\varphi + p^2/(4m_\varphi)]}, \quad (4.22)$$

the center-of-mass spatial momentum cannot be larger than $p^2 \sim 4m_\varphi T$. The momenta of the decay products must sum up as $\mathbf{q} + \mathbf{r} = \mathbf{p}$. Then at least one of them must be of the same order as p , say $q \sim 2\sqrt{m_\varphi T}$. But given that $m_\varphi \gg \pi T$, this implies that $q \gg \pi T \gg m_W, m_{E2}$. In this domain, the Standard Model particles are pole-like (see below), with energies $q_0 \approx q + m_\infty^2/(2q) \approx q$, where m_∞ corresponds to the asymptotic mass of each channel (cf. fig. 1 on p. 11). However, having $q_0 \approx q \sim 2\sqrt{m_\varphi T}$ is not enough: the two

energies must sum into the much larger $2m_\varphi \gg 2\sqrt{m_\varphi T}$. From this conflict we conclude that *both* momenta must be much *larger* than $\sim 2\sqrt{m_\varphi T}$, and back-to-back, so that there is a cancellation between them. All in all, these arguments indicate that

$$q \sim m_\varphi \gg \pi T, \quad q_0 - q \sim \frac{m_\infty^2}{m_\varphi} \ll q. \quad (4.23)$$

Adopting the power counting from eq. (4.23), let us first consider the contribution from charged gauge bosons (WW). The starting point is eq. (3.56), but multiplied with a factor 2, and with $\mathcal{F}^{\text{T,E}} \rightarrow \mathcal{G}^{\text{T,E}}$, where the resummed propagators are from eqs. (3.16)–(3.18). Denoting

$$R \equiv P - Q, \quad (4.24)$$

the result can be written in the form

$$\begin{aligned} \text{Diagram} & \quad \Pi_{K;\varphi} \stackrel{(3.56)}{\supset}_{Z \rightarrow W} \kappa^2 \Delta_{-K-P;\tilde{\varphi}}^{-1} \Delta_{P;h}^{-2} \left\{ \right. \\ & \quad \stackrel{(a)}{+} (P^2 - Q^2 - R^2)^2 \widehat{\mathcal{G}}_Q^{\text{E}} \widehat{\mathcal{G}}_R^{\text{E}} \\ & \quad \stackrel{(b)}{+} 8m_W^2 Q_\mu Q_\nu \mathbb{R}_{\mu\nu}^{\text{T}} \widehat{\mathcal{G}}_Q^{\text{E}} (\mathcal{G}_R^{\text{T}} - \mathcal{G}_R^{\text{E}}) \\ & \quad \stackrel{(c)}{+} 4m_W^4 (\mathbb{Q}_{\mu\nu}^{\text{T}} \mathbb{R}_{\mu\nu}^{\text{T}} - 2) (\mathcal{G}_Q^{\text{T}} - \mathcal{G}_Q^{\text{E}}) (\mathcal{G}_R^{\text{T}} - \mathcal{G}_R^{\text{E}}) \\ & \quad \left. \stackrel{(d)}{+} 8m_W^4 \mathcal{G}_Q^{\text{T}} \mathcal{G}_R^{\text{T}} \right\}. \end{aligned} \quad (4.25)$$

This can be readily used in eq. (4.18), once we identify the spectral functions $\varrho_{Q,\mathcal{R}}$.

In order to find $\varrho_{Q,\mathcal{R}}$, we need to inspect the propagators in eqs. (3.16)–(3.18) in the kinematic domain of eq. (4.23). For the self-energies from eqs. (3.10) and (3.11), we find

$$\Pi_Q^{\text{T}2} \stackrel{(3.10)}{\approx}_{q_0 - q \ll q} \frac{m_{\text{E}2}^2}{2}, \quad (4.26)$$

$$\widehat{\Pi}_Q^{\text{E}2} \stackrel{(3.11)}{\approx}_{q_0 - q \ll q} \frac{m_{\text{E}2}^2}{q^2} \left(1 - \frac{1}{2} \ln \frac{2q}{q_0 - q} \right). \quad (4.27)$$

This means that

$$\left\{ \mathcal{G}_Q^{\text{T}} \right\}^{-1} \stackrel{q_0 - q \ll q}{\approx} -q_0^2 + q^2 + \overbrace{m_W^2 + \frac{m_{\text{E}2}^2}{2}}^{\equiv m_{WT}^2}, \quad (4.28)$$

$$\begin{aligned} \left\{ \mathcal{G}_Q^{\text{E}} \right\}^{-1} & \stackrel{q_0 - q \ll q}{\approx} (-q_0^2 + q^2) \left[1 + \frac{m_{\text{E}2}^2}{q^2} \left(1 - \frac{1}{2} \ln \frac{2q}{q_0 - q} \right) \right] + m_W^2 \\ & \stackrel{q \gg m_{\text{E}2}}{\approx} -q_0^2 + q^2 + m_W^2. \end{aligned} \quad (4.29)$$

This in turn implies that at leading order,

$$\varrho_Q^T \equiv \text{Im } \mathcal{G}_Q^T \stackrel{(4.8), (4.28)}{\underset{q_0 - q \ll q}{\approx}} \frac{\pi \delta(q_0 - \epsilon_{WT}^q)}{2\epsilon_{WT}^q}, \quad \epsilon_{WT}^q \equiv \sqrt{q^2 + m_{WT}^2}, \quad (4.30)$$

$$\varrho_Q^E \equiv \text{Im } \mathcal{G}_Q^E \stackrel{(4.8), (4.29)}{\underset{q_0 - q \ll q}{\approx}} \frac{\pi \delta(q_0 - \epsilon_W^q)}{2\epsilon_W^q}, \quad \epsilon_W^q \equiv \sqrt{q^2 + m_W^2}. \quad (4.31)$$

The difference between eqs. (4.30) and (4.31), and thus the absence of thermal corrections in the longitudinal channel, is a consequence of the fact that the HTL correction appears as a multiplicative rather than additive factor in eq. (4.29). For the same reason, up to corrections suppressed by $\mathcal{O}(m_{E2}^2/q^2)$,

$$\widehat{\varrho}_Q^E \equiv \text{Im } \widehat{\mathcal{G}}_Q^E \stackrel{(3.18)}{\underset{(4.27)}{\approx}} \varrho_Q^E. \quad (4.32)$$

A first message conveyed by eqs. (4.30) and (4.31) is that the poles in the transverse and electric channels are *not* the same. Therefore the 2nd and 3rd structures in eq. (4.25), which contain differences between the two channels, do not cancel exactly. However, their difference is small, effectively of $\mathcal{O}(m_{E2}^2/q^2)$. We return to this below. Moreover, the pole in the electric channel, which is sometimes also called the longitudinal channel (with respect to spatial momentum), does *not* experience any thermal corrections at this order (cf. eq. (4.31)).

As a next step, we need the integral from the 2nd line of eq. (4.18). This standard computation is summarized in appendix A. In the domain where the spectral functions are dominated by poles, and assuming $m_1 + m_2 < 2m_\varphi$, the result reads

$$\langle \sigma v_{\text{rel}} \rangle \stackrel{(4.18)}{\underset{(A.7)}{=}} \frac{1}{n_{\text{eq}}^2} \frac{1}{\pi(4\pi)^4} \int_0^\infty dp p \int_{\sqrt{p^2 + 4m_\varphi^2}}^\infty dp_0 e^{-\beta p_0} \sqrt{1 - \frac{4m_\varphi^2}{\mathcal{P}^2}} \int_{\epsilon_1^-}^{\epsilon_1^+} d\epsilon_1^q \Phi|_{\epsilon_2^r = p_0 - \epsilon_1^q}, \quad (4.33)$$

where ϵ_1^\pm are given by eq. (A.4), and the angle is fixed through

$$\mathbf{q} \cdot \mathbf{r} \stackrel{r = \mathbf{p} - \mathbf{q}}{=} \mathbf{q} \cdot \mathbf{p} - q^2 = \frac{p^2 - \overbrace{(\mathbf{p} - \mathbf{q})^2}^{-(\epsilon_2^r)^2} - m_2^2 - \overbrace{q^2 - m_1^2}^{-(\epsilon_1^q)^2} + m_1^2 + m_2^2}{2}. \quad (4.34)$$

For reference, we remark that if $\Phi \approx 1$ and $2m_\varphi \gg T$, then $\langle \sigma v_{\text{rel}} \rangle \approx 1/(32\pi m_\varphi^2)$.

We apply eq. (4.33) to eq. (4.25). Let us estimate the parametric magnitudes of the various contributions, in the domain of eq. (4.23). In particular, given the large values of q_0 and q , we may ask what happens at leading order in an expansion in m_1^2/m_φ^2 and m_2^2/m_φ^2 , where $p_0 \sim q \sim r \sim m_\varphi$ and $m_{1,2} \ll p \sim 2\sqrt{m_\varphi T} \ll p_0$.

We note that the projectors in the 2nd and 3rd structures in eq. (4.25) can be written as

$$Q_\mu Q_\nu \mathbb{R}_{\mu\nu}^T \stackrel{(3.9)}{=} \frac{q^2 r^2 - (\mathbf{q} \cdot \mathbf{r})^2}{r^2}, \quad (4.35)$$

$$\mathbb{Q}_{\mu\nu}^T \mathbb{R}_{\mu\nu}^T - 2 \stackrel{(3.9)}{=} \frac{q^2 \delta_{ij} - q_i q_j}{q^2} \frac{r^2 \delta_{ij} - r_i r_j}{r^2} - 2 = -\frac{q^2 r^2 - (\mathbf{q} \cdot \mathbf{r})^2}{q^2 r^2}. \quad (4.36)$$

For vanishing masses, eq. (4.34) implies that

$$\mathbf{q} \cdot \mathbf{r} \stackrel{(4.34) \text{ with } m_{1,2} \rightarrow 0}{\epsilon_1^q = q, \epsilon_2^r = p_0 - q} \longrightarrow q r - \frac{\mathcal{P}^2}{2}, \quad q^2 r^2 - (\mathbf{q} \cdot \mathbf{r})^2 \longrightarrow \mathcal{P}^2 \left(q r - \frac{\mathcal{P}^2}{4} \right). \quad (4.37)$$

If we represent eq. (A.6) as

$$q = \frac{p_0 + x p}{2}, \quad x \in (-1, +1), \quad (4.38)$$

then

$$q^2 r^2 - (\mathbf{q} \cdot \mathbf{r})^2 \stackrel{s \equiv \mathcal{P}^2}{\underset{(4.37), (4.38)}} \longrightarrow \frac{p^2 s (1 - x^2)}{4}. \quad (4.39)$$

We recall once more that

$$s \stackrel{(4.33)}{\geq} 4m_\varphi^2, \quad q^2 \sim r^2 \stackrel{(4.23)}{\sim} s, \quad p^2 \stackrel{(4.22)}{\sim} 4m_\phi T \stackrel{\pi T \ll m_\varphi}{\ll} s. \quad (4.40)$$

We can now estimate the magnitudes of the various terms in eq. (4.25). The first one yields

$$\Phi_{WW}^{(a)} = \kappa^2 \frac{(s - 2m_W^2)^2}{(s - m_h^2)^2} \stackrel{(4.40)}{\underset{m_h, m_W \ll m_\varphi}{\approx}} \kappa^2. \quad (4.41)$$

The second gives

$$\Phi_{WW}^{(b)} \stackrel{(4.35)}{\underset{(4.39)}{\sim}} \kappa^2 \frac{m_W^2 p^2 s}{(s - m_h^2)^2 r^2} \frac{m_{E2}^2}{r^2} \stackrel{(4.40)}{\underset{m_h \ll m_\varphi}{\approx}} \kappa^2 \frac{m_W^2 p^2 m_{E2}^2}{s^3}. \quad (4.42)$$

The third produces

$$\Phi_{WW}^{(c)} \stackrel{(4.36)}{\underset{(4.39)}{\sim}} \kappa^2 \frac{m_W^4 p^2 s}{(s - m_h^2)^2 q^2 r^2} \frac{m_{E2}^4}{q^2 r^2} \stackrel{(4.40)}{\underset{m_h \ll m_\varphi}{\approx}} \kappa^2 \frac{m_W^4 p^2 m_{E2}^4}{s^5}. \quad (4.43)$$

The fourth evaluates to

$$\Phi_{WW}^{(d)} = \kappa^2 \frac{8m_W^4}{(s - m_h^2)^2} \stackrel{(4.40)}{\underset{m_h \ll m_\varphi}{\approx}} \kappa^2 \frac{8m_W^4}{s^2}. \quad (4.44)$$

So we see that eq. (4.41) dominates by a large amount, and eq. (4.44) is the second most important contribution. In other words, the vacuum matrix element, given in eq. (B.8), gives a good approximation. These estimates can be confirmed numerically, as illustrated in fig. 2. The corresponding unresummed results for all channels can be found in appendix B, whereas resummed results for the ZZ and $t\bar{t}$ channels are collected in appendices C and D, respectively, with numerical plots shown in figs. 5 (on p. 30) and 6 (on p. 32).

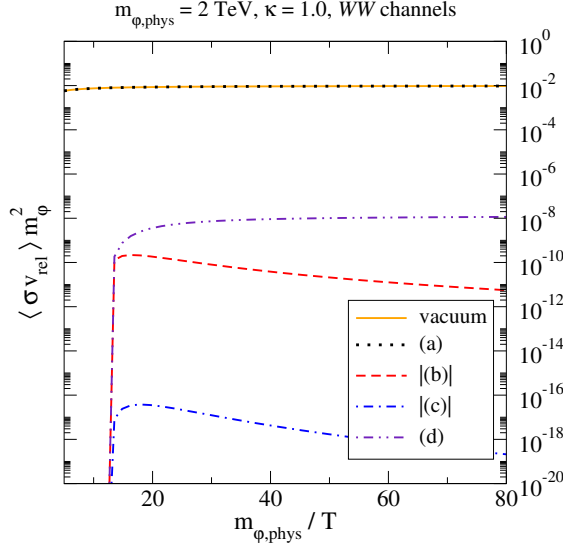


Figure 2: An illustration of the cross sections originating from the various terms in eq. (4.25), for the benchmark values $m_{\phi,\text{phys}} = 2 \text{ TeV}$, $\kappa = 1.0$. The notation “|(b)|” indicates that this channel gives a negative contribution, and we show the absolute value. The channels (b)–(d) give a vanishing contribution as we go to $T > T_c$, where $m_W^2 \rightarrow 0$.

5. Phenomenological determination of dark matter abundance

The averaged annihilation cross section that we have determined for the WW channel in sec. 4, and for the other channels in appendices B–D, yields the dark matter relic density according to eq. (2.7). For a practical integration, it is helpful to replace the physical time as an integration variable through $x \equiv \ln(T_{\text{max}}/T)$, where the choice of T_{max} is a matter of convention (it has no influence).⁴ The Jacobian between t and x follows from the Friedmann equations, yielding $dx/dt = 3c_s^2 H$, where $c_s^2 = \partial p/\partial e$ is the speed of sound squared. The number densities are conveniently normalized to the entropy density, s , and we denote $Y_\phi \equiv n_\phi/s$ and $Y_{\text{eq}} \equiv n_{\text{eq}}/s$. Then eq. (2.7) is converted into

$$\partial_x Y_\phi \stackrel{(2.7)}{\approx} -\frac{\langle \sigma v_{\text{rel}} \rangle s}{3c_s^2 H} (Y_\phi^2 - Y_{\text{eq}}^2). \quad (5.1)$$

The current energy fraction in the singlet scalar particles, compared with the observational value, $\Omega_{\text{dm}} h^2 \approx 0.120$, can be expressed as $\Omega_\phi/\Omega_{\text{dm}} \approx 2.29 (m_{\phi,\text{phys}}/\text{eV}) Y_\phi(x_0)$, where x_0 refers to the present universe. For the thermodynamic functions s , c_s^2 , and e (the last one determines the Hubble rate via $H^2 = 8\pi G e/3$), we employ the tabulations in ref. [48], and

⁴In the literature, the variable $z = m_\phi/T$ is frequently employed, but it is less convenient than our x , given that m_ϕ depends on temperature, via v and an explicit thermal correction (cf. eq. (3.3)). To use it properly would require the determination of an associated Jacobian.

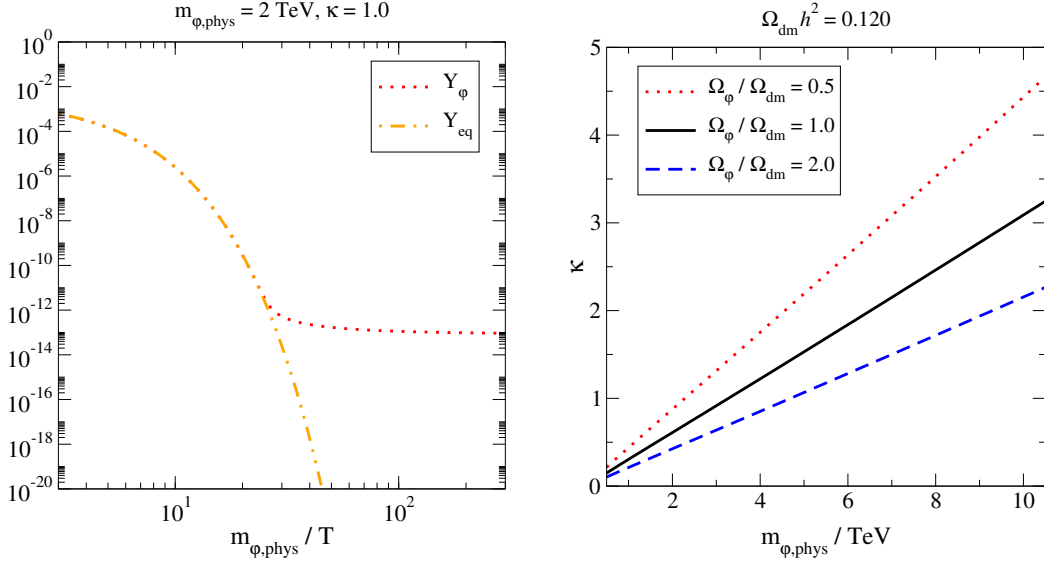


Figure 3: Left: The solution of eq. (5.1) for the benchmark values $m_{\varphi,\text{phys}} = 2 \text{ TeV}$, $\kappa = 1.0$. Right: $\Omega_\varphi / \Omega_{\text{dm}}$ in the plane of $m_{\varphi,\text{phys}}$ and κ . Within the plot resolution, the results agree with refs. [21, 23].

for the running couplings and masses of the Standard Model, the multiloop values obtained in ref. [49], see in particular the explanation in a paragraph below its eq. (4.12).

Let us briefly comment on the running of the coupling κ that connects the singlet scalar to the Standard Model (cf. eq. (3.1)). Assuming that κ is much larger than λ_φ and the Standard Model quartic coupling λ_h , the $\overline{\text{MS}}$ coupling in principle runs as

$$\bar{\mu} \frac{d\kappa(\bar{\mu})}{d\bar{\mu}} \supset \frac{\kappa^2(\bar{\mu})}{4\pi^2} \Rightarrow \kappa(\bar{\mu}) \simeq \frac{4\pi^2}{\ln(\Lambda/\bar{\mu})}, \quad (5.2)$$

where Λ is an integration constant (“Landau pole”). However, our physics takes place in the non-relativistic regime, $\pi T, \sqrt{m_\varphi T} \ll m_\varphi$. Therefore the UV energy scale that fixes $\bar{\mu}$, stays put around the rest mass, $\bar{\mu} \sim m_\varphi$, and we do not need to run κ in practice.

As an example of a solution, our benchmark displayed in figs. 2, 4, 5 and 6, namely $m_{\varphi,\text{phys}} = 2 \text{ TeV}$ and $\kappa = 1.0$, yields $Y_\varphi(x_0) \approx 8.48 \times 10^{-14}$ and $\Omega_\varphi / \Omega_{\text{dm}} \approx 0.388$, if we integrate all the way to the QCD scale ($T \sim 0.2 \text{ GeV}$, $m_{\varphi,\text{phys}}/T \sim 10^4$). The early part of the corresponding solution is illustrated in fig. 3(left).

Subsequently, we scan the singlet scalar mass between 0.5 and 10.5 TeV. The dependence of the final results on the dark matter mass and the coupling κ is shown in fig. 3(right). Even though several technical details of the analysis are different, the results agree numerically with refs. [21, 23]. To be concrete, as a specific benchmark, ref. [23] cites $\Omega_\varphi h^2 = 0.1131$ for $m_{\varphi,\text{phys}} = 9.79 \text{ TeV}$ and $\kappa = 3.1$. We obtain $\Omega_\varphi h^2 \approx 0.114$ for the same κ , and $\kappa \approx 3.12$

for the same $\Omega_\varphi h^2$, even if it has to be remarked that unfortunately the freeze-out dynamics takes place mostly in the “easy” $T > T_c$ domain for this benchmark.

If, in contrast, we go towards singlet scalar masses below 0.5 TeV, it is clear that thermal corrections become increasingly important. Most simply, this can be seen by considering temperatures $T > 2m_{\varphi,\text{phys}} \sim 1$ TeV. In the freeze-out scenario, we would think that such temperatures are “not important”, as dark matter should be well equilibrated. However, as seen from fig. 1, many asymptotic masses are larger than 0.5 TeV in this situation. Therefore, the $2 \rightarrow 2$ channel gets partly closed; more generally, the kinematics that we have assumed gets modified. To carry out a proper computation, including the initial equilibration, requires a more complicated analysis than here, with thermal mass corrections playing an $O(1)$ role.

6. Conclusions

When we dream about finding dark matter through direct or indirect detection, or collider experiments, we necessarily focus on the Standard Model particles that participate in these reactions, because they are what we have access to. In contrast, in cosmology, it is rather the inclusive annihilation cross section of the initial-state dark-matter particles that is important: in principle it does not matter in which precise way the energy released is distributed. Nevertheless, it may still be interesting to *ask* what actually happens, and this is the angle of approach that we have pursued in the current paper. In particular, we have determined the thermally averaged singlet scalar annihilation cross section by taking into account the full structures predicted by Hard Thermal Loop effective theories on the Standard Model side.

On the qualitative level, the results of our analysis can be understood from the cross sections in the WW -channel, sketched in eqs. (4.41)–(4.44). The dominant process is represented by eq. (4.41), which is independent of both the temperature and the Higgs mechanism. The largest correction is the vacuum one in eq. (4.44), induced by the Higgs mechanism. Thermal effects appear as “power corrections”: according to eqs. (4.42) and (4.43), they are proportional to the 2nd or 4th power of the Debye mass, which in turn is proportional to the gauge coupling times the temperature (cf. eq. (3.12)). However, these corrections are very much suppressed, as is visible in the numerical results in fig. 2. Consequently, the final phenomenological results, displayed in fig. 3, agree well with the literature, in which no Hard Thermal Loop resummation was implemented. We remark in passing that if one would nevertheless like to pursue higher-order corrections, it would be recommendable to return to the unifying theoretical framework mentioned in the introduction, as otherwise the analysis becomes exceedingly complicated.

Even if Hard Thermal Loop resummation had little influence on the final results of our computation, it may play a more substantial role for physics in which the large external scale of our problem, m_φ , is absent. Within the singlet scalar model itself, this could happen if we

reduce $m_{\varphi,\text{phys}}$ below 0.5 TeV, whereby the coupling κ is becoming weak (cf. fig. 3(right), and the discussion at the end of sec. 5). For very small κ , the question of the initial equilibration of φ needs to be raised, meaning that we could eventually enter the domain of the “freeze-in” mechanism (cf., e.g., ref. [50]). The diagrams that we considered in sec. 3 are a subset of those relevant for such scenarios, however the kinematics of sec. 4 cannot be simplified in the same way as in the current study, and in addition $1 \leftrightarrow 2$ processes and their LPM resummation needs to be included. In this situation thermal effects are expected to dominate the physics. Other general problems in which soft-scale physics around the electroweak crossover can be important, are low-scale leptogenesis, taking place close to when the sphaleron rate switches off [51], or the real-time physics that is associated with a first-order electroweak phase transition, present in many extensions of the Standard Model. We hope that the full set of HTL-resummed propagators and mixings that we have assembled together (cf. sec. 3.1) may facilitate studies in such contexts.

A. Two-particle phase space integral

In this appendix, we recall the evaluation of the integral from the 2nd line of eq. (4.18). To simplify the notation, we do this for two free spectral functions with different masses,

$$\begin{aligned} J_{12} &\equiv \int_{\mathbf{q}, \mathbf{r}} \int_{-\infty}^{\infty} \frac{dq_0}{\pi} \int_{-\infty}^{\infty} \frac{dr_0}{\pi} \delta^{(4)}(\mathcal{P} - \mathcal{Q} - \mathcal{R}) \frac{\pi \delta(q_0 - \epsilon_1^q)}{2\epsilon_1^q} \frac{\pi \delta(r_0 - \epsilon_2^r)}{2\epsilon_2^r} \\ &= \int_{\mathbf{q}, \mathbf{r}} \frac{\delta(p_0 - \epsilon_1^q - \epsilon_2^r) \delta^{(3)}(\mathbf{p} - \mathbf{q} - \mathbf{r})}{4\epsilon_1^q \epsilon_2^r} = \frac{1}{(2\pi)^3} \int_{\mathbf{q}} \frac{\delta(p_0 - \epsilon_1^q - \epsilon_2^{pq})}{4\epsilon_1^q \epsilon_2^{pq}}. \end{aligned} \quad (\text{A.1})$$

This is closely related to the integral in eq. (4.14), except that the masses are non-degenerate, and the result is smaller by $1/(2\pi)^4$.

Extremizing the argument of the Dirac- δ with respect to q , we find that

$$\min(\epsilon_1^q + \epsilon_2^{pq}) = \sqrt{p^2 + (m_1 + m_2)^2}. \quad (\text{A.2})$$

The energy p_0 has to be larger than this, in order for the energy constraint to be realized. To determine the range of q in which this happens, we vary the angle between \mathbf{q} and \mathbf{p} , requiring

$$\sqrt{q^2 + m_1^2} + \sqrt{(q - p)^2 + m_2^2} < p_0 < \sqrt{q^2 + m_1^2} + \sqrt{(q + p)^2 + m_2^2}. \quad (\text{A.3})$$

This leads to a minimal and maximal q , denoted by q_{\pm} , in analogy with eq. (4.15). It is helpful to express the outcome in terms of ϵ_1^q , denoting $\epsilon_1^{\pm} \equiv \epsilon_1^{q_{\pm}}$. We find

$$\epsilon_1^{\pm} = \frac{p_0 (\mathcal{P}^2 + m_1^2 - m_2^2) \pm p \sqrt{\lambda(\mathcal{P}^2, m_1^2, m_2^2)}}{2\mathcal{P}^2}, \quad (\text{A.4})$$

where the Källén function is defined as

$$\sqrt{\lambda}(x, m_1^2, m_2^2) \equiv \sqrt{x^2 + m_1^4 + m_2^4 - 2x(m_1^2 + m_2^2) - 2m_1^2 m_2^2}. \quad (\text{A.5})$$

For equal masses, eq. (A.4) reduces to eq. (4.15), and for $m_1^2, m_2^2 \ll \mathcal{P}^2$, to

$$\epsilon_1^{\pm} \approx \frac{p_0 \pm p}{2}. \quad (\text{A.6})$$

Carrying out the angular integral, the Jacobian yields $\epsilon_2^{pq}/(pq)$. Combining these steps, we find

$$J_{12} = \frac{\theta(p_0 - \sqrt{p^2 + (m_1 + m_2)^2})}{(2\pi)^4} \int_{\epsilon_1^-}^{\epsilon_1^+} \frac{d\epsilon_1^q}{8\pi p}, \quad (\text{A.7})$$

generalizing on eq. (4.17).

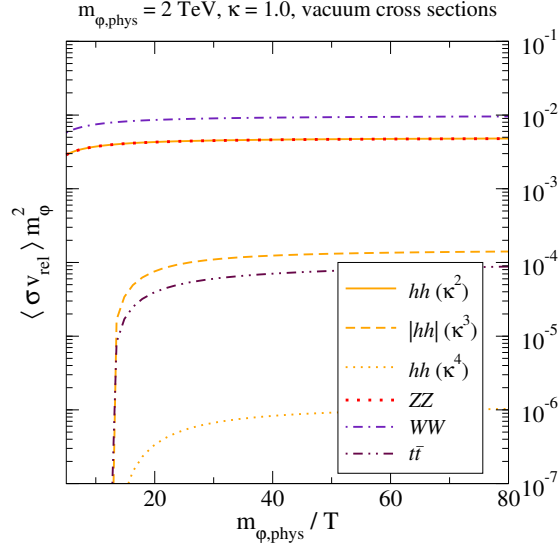


Figure 4: An illustration of the cross sections following from eqs. (B.1), (B.2), (B.3), (B.7), (B.8) and (B.9), for the benchmark values $m_{\phi,\text{phys}} = 2 \text{ TeV}$, $\kappa = 1.0$. The notation “ $|hh|$ ” indicates that this channel gives a negative contribution, and we show the absolute value. The $b\bar{b}$ channel is obtained from eq. (B.9) with $m_t \rightarrow m_b$ but is too small to be visible.

B. Leading-order matrix elements squared in the unresummed limit

For completeness, we tabulate here the matrix elements squared pertinent to the unresummed limit in the Higgs phase ($T < T_c$), using a normalization that can be directly inserted in eq. (4.33). The corresponding result for the high-temperature phase ($T > T_c$) can be found in eq. (4.19), and reads $\Phi_{\phi\phi} = 2\kappa^2$. The results are illustrated numerically in fig. 4.

Employing the Mandelstam variables s, t, u , we consider first the Higgs contributions from eqs. (3.43)–(3.45). They yield

$$\Phi_{hh} \supset \frac{\kappa^2}{2} \left\{ 1 + \frac{6m_h^2}{s - m_h^2} + \frac{9m_h^4}{(s - m_h^2)^2} \right\} = \frac{\kappa^2}{2} \frac{(s + 2m_h^2)^2}{(s - m_h^2)^2}. \quad (\text{B.1})$$

For the Higgs effects of $\mathcal{O}(\kappa^3)$ from eqs. (3.46)–(3.47), we find

$$\Phi_{hh} \supset \kappa^3 v^2 \left\{ \frac{2}{t - m_\phi^2} + \frac{6m_h^2}{(t - m_\phi^2)(s - m_h^2)} \right\} = 2\kappa^3 v^2 \frac{s + 2m_h^2}{(t - m_\phi^2)(s - m_h^2)}. \quad (\text{B.2})$$

By a renaming of integration variables, this could be symmetrized under $t \leftrightarrow u$, however this does not simplify the expression. The Higgs effects of $\mathcal{O}(\kappa^4)$ from eqs. (3.48)–(3.49) produce

$$\Phi_{hh} \supset \kappa^4 v^4 \left\{ \frac{1}{(t - m_\phi^2)^2} + \frac{1}{(t - m_\phi^2)(u - m_\phi^2)} \right\}, \quad (\text{B.3})$$

which can be written in many equivalent forms, by making use of $s + t + u = 2(m_h^2 + m_\varphi^2)$, as well as the symmetry $t \leftrightarrow u$.

For a practical integration, we note that in eq. (4.33), only the center-of-mass momentum, \mathcal{P} , and a final-state energy, ϵ_1^q , appear as integration variables. To turn eqs. (B.2) and (B.3) into a form in which we can use the same integration measure, we have to integrate over the initial-state momenta \mathbf{k} and $\mathbf{h}_{\tilde{\varphi}}$ (cf. eq. (4.20)), appearing in t or u . The Boltzmann weight, which breaks Lorentz invariance, only contains p_0 in the non-relativistic regime, not the initial-state energies separately. Therefore the average over \mathbf{k} and $\mathbf{h}_{\tilde{\varphi}}$ can be expressed as a Lorentz-invariant integral over \mathcal{K} and \mathcal{H} , depending on the invariants \mathcal{P}^2 , $\mathcal{P} \cdot \mathcal{Q}$, and \mathcal{Q}^2 . This integral can be conveniently carried out in the frame $\mathbf{q} = \mathbf{0}$, and subsequently re-expressed in a covariant form. After a tedious computation, this implies that we can effectively substitute [20]

$$\Phi_{hh} \rightarrow \frac{\kappa^2}{2} \left\{ \frac{(s + 2m_h^2)^2}{(s - m_h^2)^2} - \frac{8\kappa v^2(s + 2m_h^2)F(\xi)}{(s - m_h^2)(s - 2m_h^2)} + \frac{8\kappa^2 v^4}{(s - 2m_h^2)^2} \left[\frac{1}{1 - \xi^2} + F(\xi) \right] \right\}, \quad (\text{B.4})$$

$$\xi \equiv \frac{s}{s - 2m_h^2} \sqrt{1 - \frac{4m_h^2}{s}} \sqrt{1 - \frac{4m_\varphi^2}{s}}, \quad F(\xi) \equiv \frac{\text{artanh } \xi}{\xi}. \quad (\text{B.5})$$

Turning to gauge effects from eq. (3.56), we note that if we omit resummation, i.e. set the self-energies to zero in eqs. (3.28)–(3.30), then

$$\mathcal{F}_P^T \xrightarrow{\Pi_P^{\text{Ti}} \rightarrow 0} \Delta_{P;Z}^{-1}, \quad \mathcal{F}_P^E \xrightarrow{\Pi_P^{\text{Ei}} \rightarrow 0} \Delta_{P;Z}^{-1}, \quad \widehat{\mathcal{F}}_P^E \xrightarrow{\widehat{\Pi}_P^{\text{Ei}} \rightarrow 0} \Delta_{P;Z}^{-1}. \quad (\text{B.6})$$

Then only the first and last term of eq. (3.56) remain. Adding the contribution from the charged gauge bosons, this yields

$$\Phi_{ZZ} = \frac{\kappa^2}{2} \frac{(s - 2m_Z^2)^2 + 8m_Z^4}{(s - m_h^2)^2}, \quad (\text{B.7})$$

$$\Phi_{WW} = \kappa^2 \frac{(s - 2m_W^2)^2 + 8m_W^4}{(s - m_h^2)^2}. \quad (\text{B.8})$$

Finally, the quark contribution from eq. (3.57) turns into

$$\Phi_{t\bar{t}} = 2\kappa^2 m_t^2 N_c \frac{s - 4m_t^2}{(s - m_h^2)^2}. \quad (\text{B.9})$$

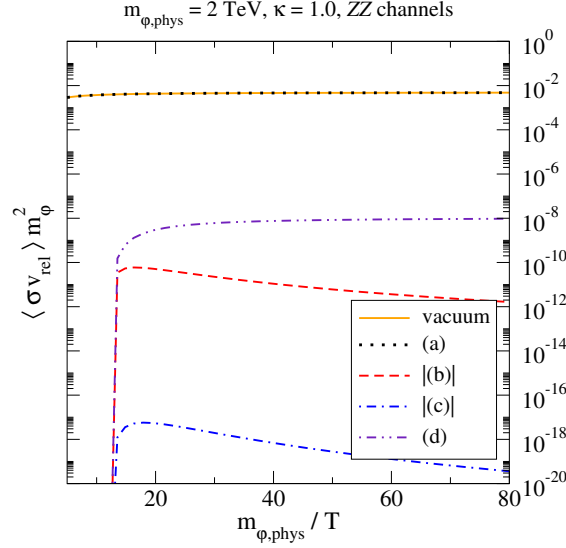


Figure 5: An illustration of the cross sections following from the various terms in eq. (3.56), for the benchmark values $m_{\phi,\text{phys}} = 2 \text{ TeV}$, $\kappa = 1.0$. The notation “|(b)|” indicates that this channel gives a negative contribution, and we show the absolute value.

C. HTL-resummed ZZ channel

We repeat here the analysis of sec. 4.4 for the ZZ channel, whose matrix element squared was given in eq. (3.56). The results are illustrated numerically in fig. 5.

The starting point is to generalize the propagators \mathcal{G}_Q^T and \mathcal{G}_Q^E , appearing in eqs. (4.28) and (4.29), into the corresponding \mathcal{F}_Q^T and \mathcal{F}_Q^E , defined according to eqs. (3.28) and (3.29), respectively. For \mathcal{F}_Q^E (and $\hat{\mathcal{F}}_Q^E$), the task is simple, because according to eq. (4.27) the self-energies $\hat{\Pi}_Q^{Ei}$ are small in the kinematic domain of interest. Therefore, following eqs. (4.31) and (4.32), we find vacuum-like spectral functions in the E channel,

$$\text{Im } \hat{\mathcal{F}}_Q^E \stackrel{(3.30)}{\approx} \text{Im } \mathcal{F}_Q^E \stackrel{(3.29)}{\approx} \frac{\pi \delta(q_0 - \epsilon_Z^q)}{2\epsilon_Z^q}, \quad \epsilon_Z^q \equiv \sqrt{q^2 + m_Z^2}. \quad (\text{C.1})$$

The situation is more complicated in the T channel, where the thermal self-energy correction is of the same order as the vacuum mass, cf. eq. (4.26). Employing Euclidean conventions for notational simplicity, the propagator is

$$\mathcal{F}_Q^T \stackrel{(3.28)}{\approx} \frac{Q^2 + \frac{1}{2}(c^2 m_{E1}^2 + s^2 m_{E2}^2)}{(Q^2 + \frac{1}{2} m_{E1}^2)(Q^2 + \frac{1}{2} m_{E2}^2) + m_Z^2 [Q^2 + \frac{1}{2}(c^2 m_{E1}^2 + s^2 m_{E2}^2)]}. \quad (\text{C.2})$$

Searching for the poles, which we parametrize through

$$m_{ZT^\pm}^2 \equiv \frac{1}{2} \left[m_Z^2 + \frac{1}{2}(m_{E1}^2 + m_{E2}^2) \right]$$

$$\pm \sqrt{m_Z^4 + m_Z^2(c^2 - s^2)(m_{E2}^2 - m_{E1}^2) + \frac{1}{4}(m_{E2}^2 - m_{E1}^2)^2} \Big] , \quad (\text{C.3})$$

the propagator may be partially fractioned,

$$\mathcal{F}_Q^T \stackrel{(\text{C.2})}{=} \stackrel{(\text{C.3})}{=} \frac{c_{ZT}^2}{Q^2 + m_{ZT+}^2} + \frac{s_{ZT}^2}{Q^2 + m_{ZT-}^2} . \quad (\text{C.4})$$

Here we have defined

$$c_{ZT}^2 \equiv \frac{1}{m_{ZT+}^2 - m_{ZT-}^2} \left[m_{ZT+}^2 - \frac{1}{2}(c^2 m_{E1}^2 + s^2 m_{E2}^2) \right] , \quad (\text{C.5})$$

$$s_{ZT}^2 \equiv \frac{1}{m_{ZT+}^2 - m_{ZT-}^2} \left[\frac{1}{2}(c^2 m_{E1}^2 + s^2 m_{E2}^2) - m_{ZT-}^2 \right] . \quad (\text{C.6})$$

These “residues” sum to unity,

$$\begin{aligned} & c_{ZT}^2 + s_{ZT}^2 \\ &= \frac{1}{m_{ZT+}^2 - m_{ZT-}^2} \left[m_{ZT+}^2 - \frac{1}{2}(c^2 m_{E1}^2 + s^2 m_{E2}^2) + \frac{1}{2}(c^2 m_{E1}^2 + s^2 m_{E2}^2) - m_{ZT-}^2 \right] \\ &= 1 , \end{aligned} \quad (\text{C.7})$$

so that they may be interpreted as thermally modified trigonometric weights squared.

For the spectral function, it follows from eq. (C.4) that

$$\text{Im } \mathcal{F}_Q^T \stackrel{(\text{C.4})}{\approx} \frac{\pi}{2} \left[c_{ZT}^2 \frac{\delta(q_0 - \epsilon_{ZT+}^q)}{\epsilon_{ZT+}^q} + s_{ZT}^2 \frac{\delta(q_0 - \epsilon_{ZT-}^q)}{\epsilon_{ZT-}^q} \right] , \quad \epsilon_{ZT\pm}^q \equiv \sqrt{q^2 + m_{ZT\pm}^2} . \quad (\text{C.8})$$

When we insert this into eq. (3.56), we obtain contributions of the same types as analyzed in eqs. (4.41)–(4.44), however with each transverse pole splitting into two separate contributions, according to eq. (C.8). The power counting employed in eqs. (4.41)–(4.44) remains valid, and therefore the transverse channel gives subdominant contributions to eq. (3.56).

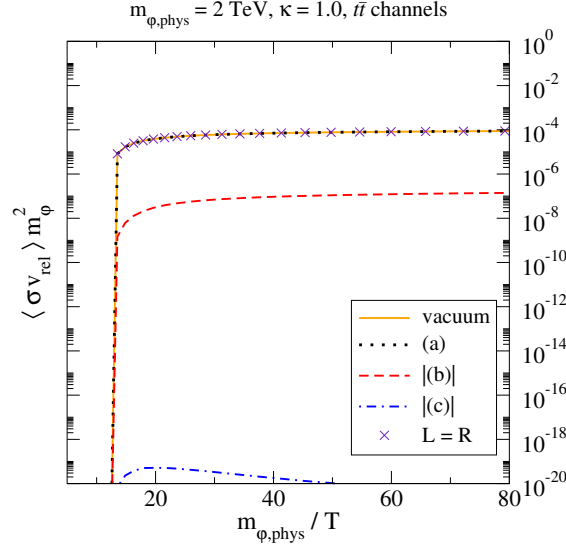


Figure 6: An illustration of the cross sections following from the various terms in eq. (3.57), with the terms split up and labelled according to eq. (D.15). We have employed the benchmark values $m_{\phi,\text{phys}} = 2 \text{ TeV}$, $\kappa = 1.0$. The notation “|(b)|” indicates that this channel gives a negative contribution, and we show the absolute value. The case (d) is not shown due to its smallness, whereas $L = R$ illustrates the outcome of the simplified expression in eq. (3.58).

D. HTL-resummed $t\bar{t}$ channel

We repeat here the analysis of sec. 4.4 for the $t\bar{t}$ channel, whose matrix element squared was given in eq. (3.57). The results are illustrated numerically in fig. 6. The common prefactor $-2\kappa^2 m_t^2 N_c \Delta_{-K-P;\bar{\phi}}^{-1} \Delta_{P;h}^{-2}$ is not shown, as we focus on the part $\mathcal{F}_Q^t \mathcal{F}_{Q-P}^t \{ \dots \}$.

To get started, we need the self-energies from eqs. (3.34) and (3.35). In the kinematic domain of eq. (4.23), these can be approximated as

$$c_{Q;t_L}^W \approx -\frac{m_{t_L}^2}{2q^2} \ln \frac{2q}{q_0 - q}, \quad (\text{D.1})$$

$$c_{Q;t_L}^P \approx \frac{m_{t_L}^2}{q^2} \left(1 - \frac{1}{2} \ln \frac{2q}{q_0 - q} \right). \quad (\text{D.2})$$

These play a role in four-vectors defined according to eq. (3.33). Even if at first sight the corrections appear small compared with the tree-level terms, the coefficients $\sim q_0, q$ in eq. (3.33) are large, so we need to be careful about when the corrections can be neglected.

Let us start by considering the propagator from eq. (3.39). Recalling that we are using

Minkowskian conventions here, the squares read

$$\begin{aligned}
L_Q^2 &= q_0^2 (1 + c_{Q;t_L}^W)^2 - q^2 (1 + c_{Q;t_L}^P)^2 \\
&\stackrel{c_{Q;t_L}^{W,P} \ll 1}{\approx} q_0^2 - q^2 + 2q_0^2 c_{Q;t_L}^W - 2q^2 c_{Q;t_L}^P \\
&\stackrel{(4.23)}{\approx}_{q_0 \approx q} q_0^2 - q^2 + 2q^2 (c_{Q;t_L}^W - c_{Q;t_L}^P) \stackrel{(D.1)}{\approx}_{(D.2)} q_0^2 - q^2 - 2m_{t_L}^2, \quad (D.3)
\end{aligned}$$

$$R_Q^2 \approx q_0^2 - q^2 - 2m_{t_R}^2, \quad (D.4)$$

$$L_Q \cdot R_Q \approx \underbrace{q_0^2 - q^2}_{\equiv Q^2} - m_{t_L}^2 - m_{t_R}^2. \quad (D.5)$$

Inserting in eq. (3.39) and factorizing the dependence on Q^2 , we find

$$\mathcal{F}_Q^t \approx \frac{1}{(Q^2 - m_{t_1}^2)(Q^2 - m_{t_2}^2)}, \quad m_{t_1}^2 \equiv m_t^2 + 2m_{t_L}^2, \quad m_{t_2}^2 \equiv m_t^2 + 2m_{t_R}^2. \quad (D.6)$$

Next, we need to tackle the numerator of eq. (3.57). In order to simplify the notation, we denote

$$\mathcal{S} \equiv Q - \mathcal{P}. \quad (D.7)$$

Also, even if there is a certain danger of confusion with the overall sign, we denote Minkowskian propagators similarly to eq. (3.41), *viz.*

$$\Delta_{Q;t_i}^{-1} \equiv \frac{1}{m_{t_i}^2 + q^2 - q_0^2} = \frac{1}{m_{t_i}^2 - Q^2}, \quad i = 1, 2, \quad (D.8)$$

where the masses are from eq. (D.6).

Let us start with the first line (\equiv (i)) of eq. (3.57). A straightforward computation yields

$$R_Q^2 L_S^2 + m_t^4 \stackrel{(D.3)}{\approx}_{(D.4)} (Q^2 - m_{t_2}^2)(\mathcal{S}^2 - m_{t_1}^2) + m_t^2 (Q^2 - m_{t_2}^2 + \mathcal{S}^2 - m_{t_1}^2) + 2m_t^4. \quad (D.9)$$

This then implies that

$$\begin{aligned}
\mathcal{F}_Q^t \mathcal{F}_S^t \{(\text{i})\} &\stackrel{(D.9)}{\approx} L_Q \cdot R_S \{ \Delta_{Q;t_1}^{-1} \Delta_{S;t_2}^{-1} - m_t^2 [\Delta_{Q;t_1}^{-1} \mathcal{F}_S^t + \Delta_{S;t_2}^{-1} \mathcal{F}_Q^t] + 2m_t^4 \mathcal{F}_Q^t \mathcal{F}_S^t \} \\
&+ R_Q \cdot L_S \{ \Delta_{Q;t_2}^{-1} \Delta_{S;t_1}^{-1} - m_t^2 [\Delta_{Q;t_2}^{-1} \mathcal{F}_S^t + \Delta_{S;t_1}^{-1} \mathcal{F}_Q^t] + 2m_t^4 \mathcal{F}_Q^t \mathcal{F}_S^t \}. \quad (D.10)
\end{aligned}$$

In a similar manner, the second line (\equiv (ii)) of eq. (3.57) yields

$$\mathcal{F}_Q^t \mathcal{F}_S^t \{(\text{ii})\} \approx \frac{m_t^2}{2} \{ \Delta_{Q;t_1}^{-1} \Delta_{S;t_1}^{-1} + \Delta_{Q;t_1}^{-1} \Delta_{S;t_2}^{-1} + \Delta_{Q;t_2}^{-1} \Delta_{S;t_1}^{-1} + \Delta_{Q;t_2}^{-1} \Delta_{S;t_2}^{-1} \}. \quad (D.11)$$

For the third line (\equiv (iii)) of eq. (3.57), we find

$$\begin{aligned}
\text{(iii)} &= 2m_t^2 (L_{\mathcal{Q}} \cdot R_{\mathcal{S}} R_{\mathcal{Q}} \cdot L_{\mathcal{S}} - L_{\mathcal{Q}} \cdot L_{\mathcal{S}} R_{\mathcal{Q}} \cdot R_{\mathcal{S}}) \\
&\stackrel{c_{\mathcal{Q};t_{L,R}}^{\text{W,P}} \ll 1}{\approx} 2m_t^2 \{ [q_0 s_0 (1 + c_{\mathcal{Q};t_L}^{\text{W}} + c_{\mathcal{S};t_R}^{\text{W}}) - \mathbf{q} \cdot \mathbf{s} (1 + c_{\mathcal{Q};t_L}^{\text{P}} + c_{\mathcal{S};t_R}^{\text{P}})] \\
&\quad \times [q_0 s_0 (1 + c_{\mathcal{Q};t_R}^{\text{W}} + c_{\mathcal{S};t_L}^{\text{W}}) - \mathbf{q} \cdot \mathbf{s} (1 + c_{\mathcal{Q};t_R}^{\text{P}} + c_{\mathcal{S};t_L}^{\text{P}})] \\
&\quad - [q_0 s_0 (1 + c_{\mathcal{Q};t_L}^{\text{W}} + c_{\mathcal{S};t_L}^{\text{W}}) - \mathbf{q} \cdot \mathbf{s} (1 + c_{\mathcal{Q};t_L}^{\text{P}} + c_{\mathcal{S};t_L}^{\text{P}})] \\
&\quad \times [q_0 s_0 (1 + c_{\mathcal{Q};t_R}^{\text{W}} + c_{\mathcal{S};t_R}^{\text{W}}) - \mathbf{q} \cdot \mathbf{s} (1 + c_{\mathcal{Q};t_R}^{\text{P}} + c_{\mathcal{S};t_R}^{\text{P}})] \} . \quad (\text{D.12})
\end{aligned}$$

The correction factors appear in different places in the two terms in eq. (D.12). However, expanding the result to linear order in them, all terms cancel. Finally, the fourth line (\equiv (iv)) of eq. (3.57) yields

$$\begin{aligned}
\mathcal{F}_{\mathcal{Q}}^t \mathcal{F}_{\mathcal{S}}^t \{(\text{iv})\} &\stackrel{(\text{D.3})}{\approx} m_t^2 L_{\mathcal{Q}} \cdot L_{\mathcal{S}} (\Delta_{\mathcal{Q};t_1}^{-1} \mathcal{F}_{\mathcal{S}}^t + \Delta_{\mathcal{S};t_1}^{-1} \mathcal{F}_{\mathcal{Q}}^t - 2m_t^2 \mathcal{F}_{\mathcal{Q}}^t \mathcal{F}_{\mathcal{S}}^t) \\
&\quad + m_t^2 R_{\mathcal{Q}} \cdot R_{\mathcal{S}} (\Delta_{\mathcal{Q};t_2}^{-1} \mathcal{F}_{\mathcal{S}}^t + \Delta_{\mathcal{S};t_2}^{-1} \mathcal{F}_{\mathcal{Q}}^t - 2m_t^2 \mathcal{F}_{\mathcal{Q}}^t \mathcal{F}_{\mathcal{S}}^t) . \quad (\text{D.13})
\end{aligned}$$

Now, we note from eqs. (D.10)–(D.13) that whenever $\mathcal{F}_{\mathcal{Q}}^t$ or $\mathcal{F}_{\mathcal{S}}^t$ appears, it is multiplied by m_t^2 . We then partial fraction

$$\begin{aligned}
m_t^2 \mathcal{F}_{\mathcal{Q}}^t &\stackrel{(\text{D.6})}{\approx} \frac{m_t^2}{(Q^2 - m_{t_1}^2)(Q^2 - m_{t_2}^2)} = \frac{m_t^2}{m_{t_1}^2 - m_{t_2}^2} \left(\frac{1}{Q^2 - m_{t_1}^2} - \frac{1}{Q^2 - m_{t_2}^2} \right) \\
&= \frac{m_t^2}{\underbrace{2(m_{t_L}^2 - m_{t_R}^2)}_{\equiv \chi_t}} (\Delta_{\mathcal{Q};t_2}^{-1} - \Delta_{\mathcal{Q};t_1}^{-1}) . \quad (\text{D.14})
\end{aligned}$$

Thereby the expressions split into a large number of terms. Though it is a bit tedious, these can be regrouped into expressions of 0th, 1st, or 2nd order in χ_t . In the end, we also note that the result is symmetric in $\mathcal{Q} \leftrightarrow \mathcal{S}$. By the substitution $\mathcal{Q} \rightarrow \mathcal{P} - \mathcal{Q}$, implying $\mathcal{Q} \rightarrow -\mathcal{S}$ and $\mathcal{S} \rightarrow -\mathcal{Q}$, terms can be combined. This produces

$$\begin{aligned}
\mathcal{F}_{\mathcal{Q}}^t \mathcal{F}_{\mathcal{S}}^t \{(\text{i-iv})\} &\stackrel{(\text{a})}{\approx} \Delta_{\mathcal{Q};t_1}^{-1} \Delta_{\mathcal{S};t_2}^{-1} (2L_{\mathcal{Q}} \cdot R_{\mathcal{S}} + m_t^2) \\
&\stackrel{(\text{b})}{+} (\Delta_{\mathcal{Q};t_1}^{-1} \Delta_{\mathcal{S};t_1}^{-1} + \Delta_{\mathcal{Q};t_2}^{-1} \Delta_{\mathcal{S};t_2}^{-1}) \frac{m_t^2}{2} \\
&\stackrel{(\text{c})}{+} 2\chi_t \Delta_{\mathcal{Q};t_1}^{-1} (\Delta_{\mathcal{S};t_2}^{-1} - \Delta_{\mathcal{S};t_1}^{-1}) (L_{\mathcal{Q}} - R_{\mathcal{Q}}) \cdot L_{\mathcal{S}} \\
&\stackrel{(\text{c})}{-} 2\chi_t \Delta_{\mathcal{Q};t_2}^{-1} (\Delta_{\mathcal{S};t_2}^{-1} - \Delta_{\mathcal{S};t_1}^{-1}) (L_{\mathcal{Q}} - R_{\mathcal{Q}}) \cdot R_{\mathcal{S}} \\
&\stackrel{(\text{d})}{+} 2\chi_t^2 (\Delta_{\mathcal{Q};t_1}^{-1} - \Delta_{\mathcal{Q};t_2}^{-1}) (\Delta_{\mathcal{S};t_2}^{-1} - \Delta_{\mathcal{S};t_1}^{-1}) (L_{\mathcal{Q}} - R_{\mathcal{Q}}) \cdot (L_{\mathcal{S}} - R_{\mathcal{S}}) . \quad (\text{D.15})
\end{aligned}$$

The labelling (a)–(d) corresponds to that shown in fig. 6.

The terms in eq. (D.15) have a certain physical interpretation. As we see from eq. (D.6), the state “ t_1 ” corresponds to left-handed chirality, the state “ t_2 ” to right-handed chirality. The term on the first line of eq. (D.15) is chirality conserving (scalar splits into left and right). The term of the second line is not (scalar into left-left or right-right), hence it is proportional to the chirality-breaking vacuum mass squared. On the third and fourth lines, the coefficient χ_t is inversely proportional to chirality breaking, cf. eq. (D.14). But there are *two* differences multiplying χ_t , which are also proportional to chirality breaking. Therefore, the terms vanish if we envisage taking the chirally symmetric limit (i.e. $g_1, g_2, h_t, h_b \rightarrow 0$, $g_3 \neq 0$). Finally, on the fifth line, the coefficient χ_t^2 is quadratically divergent in chirality breaking, but there are *four* differences, more than compensating for the singular coefficient.

Therefore, in the would-be chirally symmetric limit, the three last lines drop out. The first two lines can be combined ($m_{t_1} \rightarrow m_{t_2}$ if $L \rightarrow R$, cf. eq. (D.6)), and amount to eq. (3.58).

In order to take further steps, it is helpful to go over to the variables in eq. (4.37). For this, we write

$$\mathcal{S} \stackrel{(4.24)}{\underset{(D.7)}{=}} -\mathcal{R}, \quad (D.16)$$

which implies

$$\begin{aligned} L_{\mathcal{Q}} \cdot R_{\mathcal{S}} &\approx +q_0 s_0 (1 + c_{\mathcal{Q};t_L}^W + c_{\mathcal{S};t_R}^W) - \mathbf{q} \cdot \mathbf{s} (1 + c_{\mathcal{Q};t_L}^P + c_{\mathcal{S};t_R}^P) \\ &= -q_0 r_0 (1 + c_{\mathcal{Q};t_L}^W + c_{\mathcal{R};t_R}^W) + \mathbf{q} \cdot \mathbf{r} (1 + c_{\mathcal{Q};t_L}^P + c_{\mathcal{R};t_R}^P). \end{aligned} \quad (D.17)$$

Consider first the terms without the c -factors. We assume that the propagators have the masses m_i and m_j , and find

$$\begin{aligned} -q_0 r_0 + \mathbf{q} \cdot \mathbf{r} &= -\epsilon_i^q \epsilon_j^r + \mathbf{q} \cdot \mathbf{r} \\ &= \frac{1}{2} [-(\epsilon_i^q + \epsilon_j^r)^2 + (\epsilon_i^q)^2 + (\epsilon_j^r)^2 + (\mathbf{q} + \mathbf{r})^2 - q^2 - r^2] \\ &= -\frac{1}{2} (s - m_i^2 - m_j^2). \end{aligned} \quad (D.18)$$

Thereby

$$2L_{\mathcal{Q}} \cdot R_{\mathcal{S}} + m_t^2 \supset -(s - m_i^2 - m_j^2 - m_t^2). \quad (D.19)$$

If we add the contribution from the second line of eq. (D.15) and send $m_i, m_j \rightarrow m_t$, the vacuum matrix element squared in eq. (B.9) is recovered.

In the correction terms in eq. (D.17), which are already proportional to thermal masses

(cf. eqs. (D.1) and (D.2)), we can employ ultrarelativistic kinematics from eq. (4.37). Hence,

$$\begin{aligned}
L_{\mathcal{Q}} \cdot R_{\mathcal{S}} &\stackrel{(D.17)}{\supset} -q_0 r_0 (c_{\mathcal{Q};t_L}^W + c_{\mathcal{R};t_R}^W) + \mathbf{q} \cdot \mathbf{r} (c_{\mathcal{Q};t_L}^P + c_{\mathcal{R};t_R}^P) \\
&\stackrel{(4.37)}{\approx} -qr (c_{\mathcal{Q};t_L}^W + c_{\mathcal{R};t_R}^W) + \left(qr - \frac{s}{2}\right) (c_{\mathcal{Q};t_L}^P + c_{\mathcal{R};t_R}^P) \\
&= qr (c_{\mathcal{Q};t_L}^P - c_{\mathcal{Q};t_L}^W + c_{\mathcal{R};t_R}^P - c_{\mathcal{R};t_R}^W) - \frac{s}{2} (c_{\mathcal{Q};t_L}^P + c_{\mathcal{R};t_R}^P) \\
&\approx \frac{r m_{t_L}^2}{q} + \frac{q m_{t_R}^2}{r} - \frac{s}{2} \left[\frac{m_{t_L}^2}{q^2} \left(1 - \frac{1}{2} \ln \frac{2q}{\epsilon_i^q - q}\right) + \frac{m_{t_R}^2}{r^2} \left(1 - \frac{1}{2} \ln \frac{2r}{\epsilon_j^r - r}\right) \right].
\end{aligned} \tag{D.20}$$

This does *not* simplify in any substantial way if we take the chirally symmetric limit $L \rightarrow R$.

To summarize, in the fermionic channel, the first thermal corrections do *not* amount to simple mass modifications of vacuum cross sections, but have a more delicate structure. This remains true if we take the chirally symmetric limit $L \rightarrow R$. Nevertheless, in the domain of eq. (4.23), the mass corrections are small. This is also clearly visible from fig. 6.

References

- [1] N. Aghanim *et al* [Planck], *Planck 2018 results. VI. Cosmological parameters*, Astron. Astrophys. 641 (2020) A6; *ibid.* 652 (2021) C4 (E) [1807.06209].
- [2] B.W. Lee and S. Weinberg, *Cosmological Lower Bound on Heavy-Neutrino Masses*, Phys. Rev. Lett. 39 (1977) 165.
- [3] M. Srednicki, R. Watkins and K.A. Olive, *Calculations of relic densities in the early universe*, Nucl. Phys. B 310 (1988) 693.
- [4] K. Griest and D. Seckel, *Three exceptions in the calculation of relic abundances*, Phys. Rev. D 43 (1991) 3191.
- [5] P. Gondolo and G. Gelmini, *Cosmic abundances of stable particles: Improved analysis*, Nucl. Phys. B 360 (1991) 145.
- [6] S. Caron-Huot, *Asymptotics of thermal spectral functions*, Phys. Rev. D 79 (2009) 125009 [0903.3958].
- [7] A. Salvio, P. Lodone and A. Strumia, *Towards leptogenesis at NLO: the right-handed neutrino interaction rate*, JHEP 08 (2011) 116 [1106.2814].
- [8] M. Laine and Y. Schröder, *Thermal right-handed neutrino production rate in the non-relativistic regime*, JHEP 02 (2012) 068 [1112.1205].
- [9] S. Biondini, N. Brambilla, M.A. Escobedo and A. Vairo, *An effective field theory for non-relativistic Majorana neutrinos*, JHEP 12 (2013) 028 [1307.7680].
- [10] M. Beneke, F. Dighera and A. Hryczuk, *Relic density computations at NLO: infrared finiteness and thermal correction*, JHEP 10 (2014) 045; *ibid.* 07 (2016) 106 (E) [1409.3049].
- [11] P. Butola, D. Indumathi and P. Sen, *NLO thermal corrections to dark matter annihilation cross sections: A novel approach*, Phys. Rev. D 110 (2024) 036006 [2404.15987].
- [12] M. Laine, *Thermal right-handed neutrino production rate in the relativistic regime*, JHEP 08 (2013) 138 [1307.4909].
- [13] R.D. Pisarski, *Scattering amplitudes in hot gauge theories*, Phys. Rev. Lett. 63 (1989) 1129.
- [14] J. Frenkel and J.C. Taylor, *High-temperature limit of thermal QCD*, Nucl. Phys. B 334 (1990) 199.
- [15] E. Braaten and R.D. Pisarski, *Soft amplitudes in hot gauge theories: A general analysis*, Nucl. Phys. B 337 (1990) 569.
- [16] J.C. Taylor and S.M.H. Wong, *The effective action of hard thermal loops in QCD*, Nucl. Phys. B 346 (1990) 115.
- [17] V. Silveira and A. Zee, *Scalar Phantoms*, Phys. Lett. B 161 (1985) 136.
- [18] J. McDonald, *Gauge singlet scalars as cold dark matter*, Phys. Rev. D 50 (1994) 3637 [hep-ph/0702143].

- [19] C.P. Burgess, M. Pospelov and T. ter Veldhuis, *The Minimal Model of nonbaryonic dark matter: a singlet scalar*, Nucl. Phys. B 619 (2001) 709 [hep-ph/0011335].
- [20] W.L. Guo and Y.L. Wu, *The real singlet scalar dark matter model*, JHEP 10 (2010) 083 [1006.2518].
- [21] J.M. Cline, K. Kainulainen, P. Scott and C. Weniger, *Update on scalar singlet dark matter*, Phys. Rev. D 88 (2013) 055025; *ibid.* 92 (2015) 039906 (E) [1306.4710].
- [22] H. Wu and S. Zheng, *Scalar dark matter: real vs complex*, JHEP 03 (2017) 142 [1610.06292].
- [23] P. Athron *et al.* [GAMBIT], *Status of the scalar singlet dark matter model*, Eur. Phys. J. C 77 (2017) 568 [1705.07931].
- [24] T. Binder, T. Bringmann, M. Gustafsson and A. Hryczuk, *Dark matter relic abundance beyond kinetic equilibrium*, Eur. Phys. J. C 81 (2021) 577 [2103.01944].
- [25] T. Abe, *Early kinetic decoupling and a pseudo-Nambu-Goldstone dark matter model*, Phys. Rev. D 104 (2021) 035025 [2106.01956].
- [26] K. Ala-Mattinen, M. Heikinheimo, K. Kainulainen and K. Tuominen, *Momentum distributions of cosmic relics: Improved analysis*, Phys. Rev. D 105 (2022) 123005 [2201.06456].
- [27] S. Kim and M. Laine, *Langevin simulation of dark matter kinetic equilibration*, JCAP 05 (2023) 003 [2302.05129].
- [28] P. Maták, *Unitarity, real-intermediate states, and fixed-order approach to resonant dark matter annihilation*, Phys. Rev. D 109 (2024) 043008 [2305.19238].
- [29] J. Heisig, M. Krämer, E. Madge and A. Mück, *Probing Higgs-portal dark matter with vector-boson fusion*, JHEP 03 (2020) 183 [1912.08472].
- [30] M. Di Mauro, C. Arina, N. Fornengo, J. Heisig and D. Massaro, *Dark matter in the Higgs resonance region*, Phys. Rev. D 108 (2023) 095008 [2305.11937].
- [31] J. March-Russell, S.M. West, D. Cumberbatch and D. Hooper, *Heavy dark matter through the Higgs portal*, JHEP 07 (2008) 058 [0801.3440].
- [32] P.M. Schicho, T.V.I. Tenkanen and J. Österman, *Robust approach to thermal resummation: Standard Model meets a singlet*, JHEP 06 (2021) 130 [2102.11145].
- [33] L. Niemi, M.J. Ramsey-Musolf and G. Xia, *Nonperturbative study of the electroweak phase transition in the real scalar singlet extended standard model*, Phys. Rev. D 110 (2024) 115016 [2405.01191].
- [34] M. Escudero Abenza and T. Hambye, *The simplest dark matter model at the edge of perturbativity*, Phys. Lett. B 868 (2025) 139696 [2505.02408].
- [35] D. Bödeker and M. Laine, *Heavy quark chemical equilibration rate as a transport coefficient*, JHEP 07 (2012) 130 [1205.4987].
- [36] M. Laine, *Resonant s-channel dark matter annihilation at NLO*, JHEP 01 (2023) 157 [2211.06008].

- [37] D. Bödeker, M. Sangel and M. Wörmann, *Equilibration, particle production, and self-energy*, Phys. Rev. D 93 (2016) 045028 [1510.06742].
- [38] J. Bernstein, L.S. Brown and G. Feinberg, *Cosmological heavy-neutrino problem*, Phys. Rev. D 32 (1985) 3261.
- [39] M. D’Onofrio and K. Rummukainen, *Standard Model cross-over on the lattice*, Phys. Rev. D 93 (2016) 025003 [1508.07161].
- [40] K. Miura, Y. Hidaka, D. Satow and T. Kunihiro, *Neutrino spectral density at electroweak scale temperature*, Phys. Rev. D 88 (2013) 065024 [1306.1701].
- [41] J. Ghiglieri and M. Laine, *Neutrino dynamics below the electroweak crossover*, JCAP 07 (2016) 015 [1605.07720].
- [42] T.S. Biró and M.H. Thoma, *Damping rate and Lyapunov exponent of a Higgs field at high temperature*, Phys. Rev. D 54 (1996) 3465 [hep-ph/9603339].
- [43] M. Eriksson and M. Laine, *Soft contributions to the thermal Higgs width across an electroweak phase transition*, JCAP 06 (2024) 016 [2404.06116].
- [44] P.B. Arnold, *Phase transition temperatures at next-to-leading order*, Phys. Rev. D 46 (1992) 2628 [hep-ph/9204228].
- [45] A.D. Linde, *Infrared problem in thermodynamics of the Yang-Mills gas*, Phys. Lett. B 96 (1980) 289.
- [46] H.A. Weldon, *Effective fermion masses of order gT in high-temperature gauge theories with exact chiral invariance*, Phys. Rev. D 26 (1982) 2789.
- [47] G.F. Giudice, A. Notari, M. Raidal, A. Riotto and A. Strumia, *Towards a complete theory of thermal leptogenesis in the SM and MSSM*, Nucl. Phys. B 685 (2004) 89 [hep-ph/0310123].
- [48] M. Laine, M. Meyer and Y. Schröder, *Data for the Standard Model equation of state*, <http://laine.itp.unibe.ch/eos15/>.
- [49] M. Laine, P. Schicho and Y. Schröder, *A QCD Debye mass in a broad temperature range*, Phys. Rev. D 101 (2020) 023532 [1911.09123].
- [50] T. Bringmann, S. Heeba, F. Kahlhoefer and K. Vangsnes, *Freezing-in a hot bath: resonances, medium effects and phase transitions*, JHEP 02 (2022) 110 [2111.14871].
- [51] M. D’Onofrio, K. Rummukainen and A. Tranberg, *Sphaleron Rate in the Minimal Standard Model*, Phys. Rev. Lett. 113 (2014) 141602 [1404.3565].